npj Parkinson's Disease

https://doi.org/10.1038/s41531-026-01318-7

Article in Press

Loss of METTL14 in dopaminergic neurons disrupts ER homeostasis via m6A-dependent regulation of Atp2a3 mRNA: Implications for Parkinson's Disease

Received: 9 October 2024

Accepted: 1 March 2026

Cite this article as: Teng, Y., Liu, Z., Wei, F. *et al.* Loss of METTL14 in dopaminergic neurons disrupts ER homeostasis via m6A-dependent regulation of Atp2a3 mRNA: Implications for Parkinson's Disease. *npj Parkinsons Dis.* (2026). https://doi.org/10.1038/s41531-026-01318-7

Yan Teng, Zhihao Liu, Fan Wei, Qin Tang, Manjun Li, Xingmin Chen, Jin Yi, Shu He, Jianli Xu, Yuqing Hang, Kaifang Wang, Yanzhuo Liu, Haisong Jiang, Weidong Le & Lu Yang

Title: Loss of METTL14 in dopaminergic neurons disrupts ER homeostasis via m6A-dependent regulation of Atp2a3 mRNA: Implications for Parkinson's Disease

Authors: Yan Teng [1,2¶], Zhihao Liu [2¶], Fan Wei [2¶], Qin Tang [2¶], Manjun Li [2], Xingmin Chen [2], Jin Yi [1,2], Shu He [1,2], Jianli Xu [1,2], Yuqing Hang [2], Kaifang Wang [2], Yanzhuo Liu [2], Haisong Jiang [1,2*], Weidong Le [1,3*] and Lu Yang [1,2*]

[1] Department of Neurology & Institute of Neurology, Sichuan Provincial People's Hospital, University of Electronic Science and Technology of China, Chengdu, Sichuan 610054, China

[2] School of Medicine, University of Electronic Science and Technology of China, Chengdu, Sichuan 610054, China

3. Neurology Program , Sir Run-Run Shaw Hospital, Zhejiang University school of Medicine, Hangzhou 310016,China

[¶] These authors contributed equally to this work.

*Correspondence to Lu Yang (lyang@uestc.edu.cn), Weidong Le（wdle@sibs.ac.cn）and Haisong Jiang (jhsarchangle@hotmail.com) No.4, Section 2, North Jianshe Road, Chengdu, Sichuan 610054, China.

Abstract

Dopaminergic (DA) neurons are highly susceptible to endoplasmic reticulum (ER) burden and redox imbalance, which drive their degeneration and contribute to Parkinson's disease (PD) pathogenesis. Previous work established METTL14-mediated N6-methyladenosine (m6A) modification as critical for dopaminergic (DA) neuron survival. Here, we delineate the underlying mechanism by which m6A dysregulation triggers neurodegeneration through the post-transcriptional modulation of key target genes. Using Mettl14 conditional knockout mice, we identified the ER calcium channel ATP2A3—a key calcium homeostasis regulator and known PD biomarker—as a major target of METTL14. METTL14 deficiency significantly reduced ATP2A3 expression, thereby exacerbating ER homeostasis and oxidative stress, ultimately leading to DA neuronal death. Restoring METTL14 *in vivo* alleviates motor deficits and neurodegeneration. Our findings reveal that m6A-mediated regulation of ATP2A3 bridges RNA epigenetic dysregulation to PD pathogenesis, highlighting this axis as a potential therapeutic target in this disease.

Key words

RNA epigenetics, Dopaminergic neuron, ER stress, APT2A3, Parkinson's disease

Introduction

N6-methyladenosine (m6A) is the most prevalent modification found on eukaryotic messenger RNA (mRNA) and actively participates in post-transcriptional regulation by modulating mRNA metabolism and translation. The levels of m6A in RNA are regulated by specific enzymes, including methyltransferases and demethylases [1]. Previous research has indicated that m6A tagging may play a unique role in the adult brain, as m6A levels are relatively low during embryogenesis but drastically increase by adulthood in mouse brain tissue[2]. The m6A modification has been shown to regulate multiple neuronal functions, including synapse formation [3], axon regeneration [4], and motor activities [5]. Results from these studies also indicate that compensatory upregulation or downregulation of m6A levels may be necessary for specific neuronal cell functions, depending on the physiological or pathological state.

Dopaminergic (DA) neurons, characterized by the expression of the rate-limiting enzyme tyrosine hydroxylase (TH) to produce catecholamines, are essential for various brain functions, including voluntary movement, reward learning, and motivation[6]. The largest populations of midbrain DA neurons are localized in two neighboring nuclei, the substantia nigra (SN) and the ventral tegmental area (VTA). Dopaminergic projections also exert a widespread influence over multiple brain regions, modulating various behaviors. Excessive loss of DA neurons leads to Parkinson's disease (PD), the most common neurodegenerative

disorder characterized by the loss of nigrostriatal dopamine-producing neurons[7]. Although the exact pathogenesis of PD remains unclear, numerous studies have demonstrated that ER burden and redox imbalance are the key factors in the degeneration of DA neurons. Disruptions in the physiological maintenance of redox potential interfere with essential cellular processes, ultimately leading to neuronal death. Several mechanisms are known to generate reactive oxygen species (ROS), including dopamine metabolism, mitochondrial dysfunction, neuroinflammation, calcium dysregulation, and aging. The interplay between these mechanisms accelerates DA neuronal degeneration, highlighting ER burden and oxidative stress as a central factor in PD progression.

Several studies, including our own, have documented the association of m6A modification with DA neuron function in PD [8-13]. It has been reported that the overall m6A level in the striatum was decreased in a PD rat model [12]. Additionally, treatment with m6A inhibitors triggered oxidative stress and induced apoptosis of neurons. Moreover, inhibitors of the fat mass and obesity-associated protein (FTO), an important regulator of m6A demethylation, have been shown to support the survival of DA neurons from growth factor deprivation-induced death *in vitro* [13]. These data suggest a possible role of m6A dysregulation in DA neurons during the progression of PD. A recent study investigated the levels of m6A and its modulators, including methyltransferase like 3 (METTL3), methyltransferase like 14 (METTL14), and YTH domain-containing family protein 2 (YTHDF2), in peripheral blood mononuclear cells of patients with PD. These protein levels were significantly lower than those of healthy controls, and METTL14 was identified as the main factor involved in abnormal m6A modification in PD patients [14].

Previously, we discovered that altered expression of methyltransferase METTL14, achieved through lentivirus-mediated deletion of Mettl14 in the substantia nigra (SN) region, directly led to the loss of DA neurons in mice [11]. However, the effect of METTL14 on DA neurons needs to be further confirmed, as local injection causes changes in a variety of cells, not just neurons. More importantly, the underlying mechanism has remained elusive. In this study, we generated a conditional knockout mouse model (Mettl14-cKO) to specifically delete Mettl14 in DA neurons. The aim was to investigate the functional consequences of m6A loss in Mettl14-cKO mice and identify the precise mechanism of m6A modification in the regulation of survival and function of DA neurons.

Results

Aged Mettl14-cKO mice exhibit motor deficits

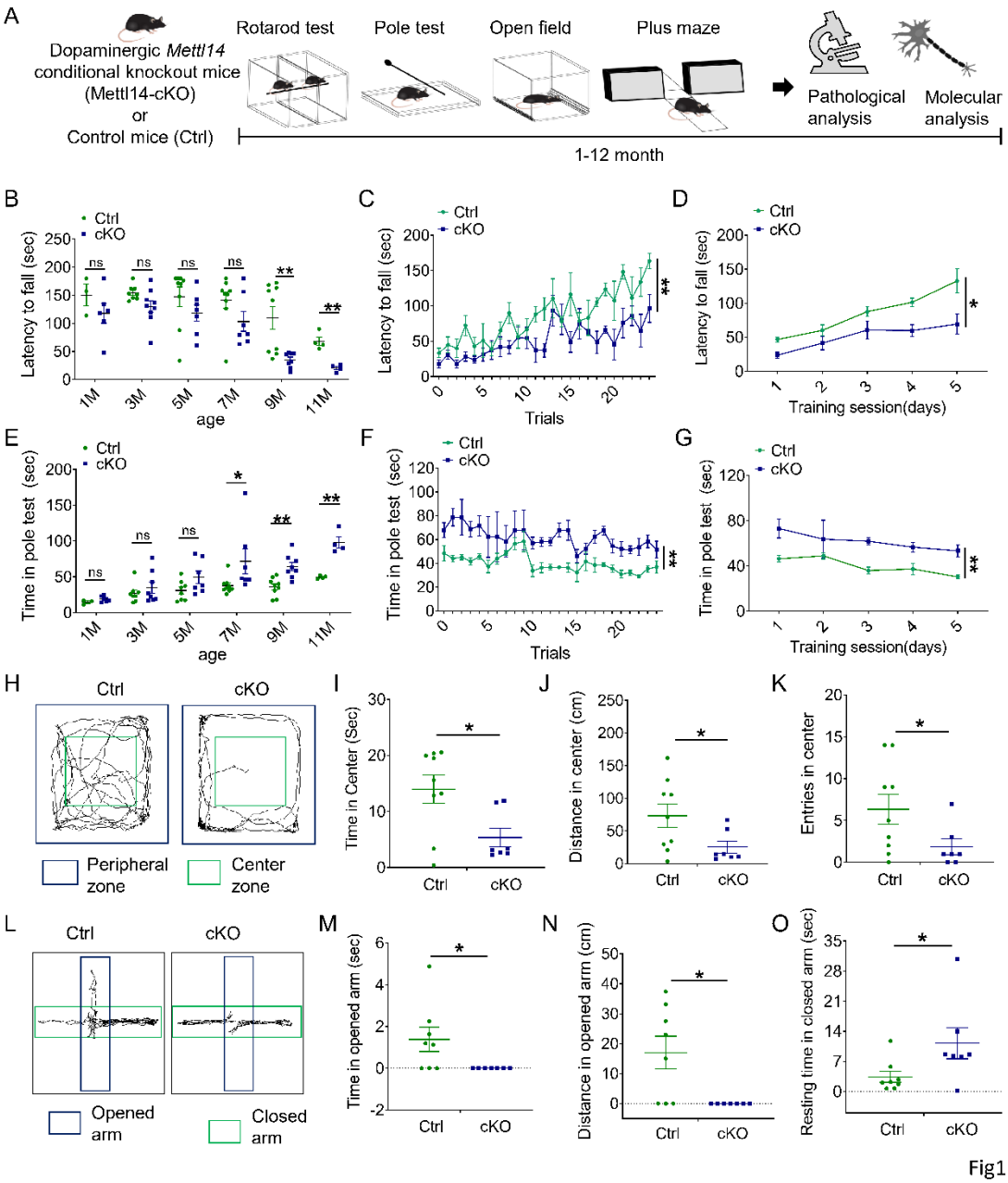

Fig1

In this study, we first examined the dynamic expression of Mettl14 in neurotoxin 1-methyl-4-phenyl-1,2,3,6-tetrahydropyridine (MPTP)-treated mice and 1-methyl-4-phenylpyridinium (MPP^+)-stimulated neurons. We found that both mRNA and protein expression of METTL14 were reduced in the SN of MPTP-treated mice (Supplementary Figure 1A-1C) and MPP^+-stimulated neurons (Supplementary Figure 1D-1I). These results further suggest that METTL14-mediated m6A plays an important role in the normal function of DA neurons. Altered METTL14 expression in DA neurons might be correlated with the dysfunction of the dopaminergic system in mice.

To investigate the regulatory function of METTL14-mediated m6A modification in DA neurons, we utilized conditional Mettl14-targeted mice with LoxP sites (Ctrl mice) [15] crossed with mice expressing Cre-recombinase under the dopamine transporter (DAT) promoter, to generate a mouse line with conditional knockout of Mettl14 in DA neurons (Mettl14-cKO mice) (Supplementary Figure 2A-2B). The conditional knockout of Mettl14 in DA neurons did not impact the body and brain weight of mice under normal feeding conditions (Supplementary Figure 2C-2E). Immunofluorescence analysis confirmed the absence of METTL14 in DAT-positive neurons in the SN region of Mettl14-cKO mice, indicating successful deletion of Mettl14 in DA neurons (Supplementary Figure 3A). We also detected reduced m6A modification in RNA of SN from Mettl14-cKO mice by dot blot assay (Supplementary Figure 3B).

Next, we evaluated the effect of Mettl14 deletion on motor function and locomotor activity of mice (Fig1.A). The results from the rotarod test indicated that the latency time of Mettl14-cKO mice was significantly reduced compared to the littermate control mice after 9 months of age (Fig1.B). Furthermore, the impaired motor function of Mettl14-cKO mice could not be improved with increased training sessions (Fig1.C-D). Similarly, the pole test showed that Mettl14-cKO mice spent significantly longer time on the pole compared to control mice after 7 months of age and could not be improved by training (Fig1.E-G).

In addition, we assessed the locomotor activity of the mice using the open field and plus maze tests. Our results showed that at 7-9 months of age, Mettl14-cKO mice spent less time and covered less distance, as well as made fewer entries into the central area of the open field compared to control mice (Fig1.H-K). Similarly, in the plus maze test, Mettl14-cKO mice spent less time and covered a shorter distance in the open arm, while the resting time spent in the closed arm was longer than the littermate controls (Fig1.L-O). These findings suggest that Mettl14 is crucial for DA neuron-mediated behavior function, Mettl14 deletion in DA neurons impairs both motor function and locomotor activity in mice.

Deletion of Mettl14 leads to degeneration of DA neurons in Mettl14-cKO mice

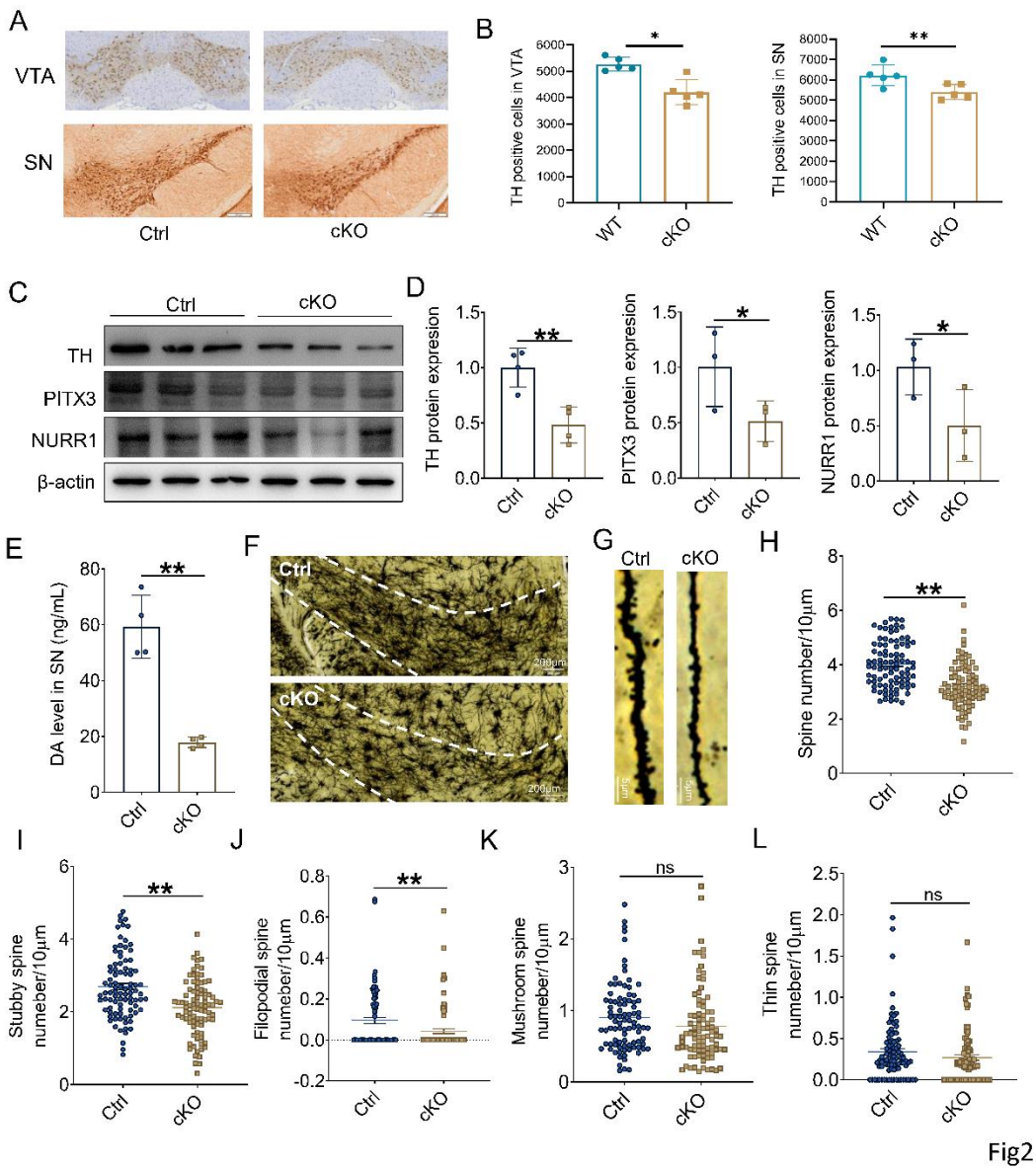

Fig2

To investigate the pathological alterations in DA neurons in the SN of Mettl14-cKO mice, we first assayed the expression of tyrosine hydroxylase (TH) in the SN of mice.TH is an enzyme necessary for dopamine neurotransmitter synthesis and serves as an important marker protein of DA neuron. We observed a significant decrease in the number of TH-positive cells in Mettl14-cKO mice compared to littermate control, as detected by stereologic analysis of DA neurons in SN and VTA region (Fig2.A-B) and immunostaining (Supplementary Figure 4).Western blot analysis also revealed reduced protein expression of TH, as well as of paired-like homeodomain transcription factor 3 (PITX3) and nuclear receptor-related 1 (NURR1), which are important transcriptional regulatory factors in DA neurons [16,17] (Fig2.C-D). Notably, ELISA assay also revealed a decrease in the level of dopamine transmitter in the SN of Mettl14-cKO mice (Fig2.E).

Available evidence suggests that the degeneration of DA neurons begins with defects in the dopaminergic synapse in the striatum, which is followed by retrograde degeneration of dopaminergic axons [18,19]. Here our

primary focus was on the integrity of DA neuron in the SN region and since we observed DA neuron loss in the SN of 9-month-old mice, we aimed to investigate whether there were early changes in spine density and morphology in the SN DA neurons. Therefore, we performed Golgi staining to examine possible alterations in neuronal dendrites and dendritic spines of Mettl14-cKO mice. Our data indicated that dendritic spine density and morphology were altered in 6-month-old Mettl14-cKO mice compared to littermate controls (Fig2.F-L). We observed a reduction in total spine number (Fig 2.H), stubby spine number (Fig2.I), and filopodial spine number (Fig2.J) on SN neurons of Mettl14-cKO mice, while the number of mushroom spine (Fig2.K) and thin spine (Fig2.L) was not affected according to the quantification analysis.

All these results indicate that METTL14 is essential for the physiological function of DA neurons and that deletion induces degeneration of DA neurons.

Altered m6A methylation and gene transcription profile in SN region of Mettl14-cKO mice

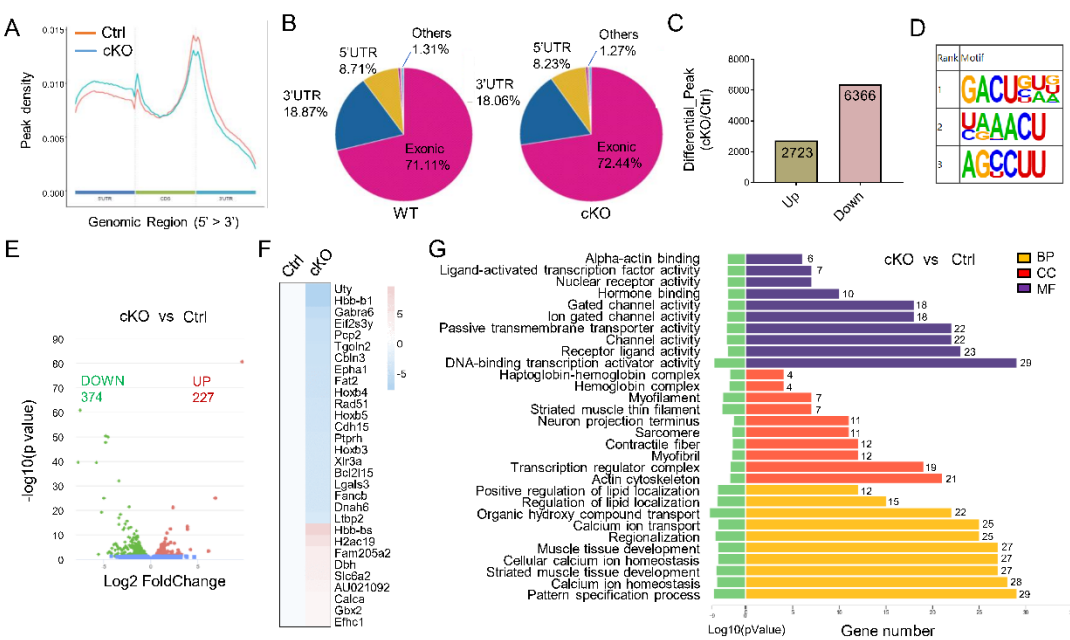

Fig3 We next aimed to explore the regulatory mechanism of METTL14-mediated m6A modification in DA neurons. We anatomically removed SN tissues from Mettl14-cKO mice and littermate controls for mRNA extraction and m6A-mRNA immunoprecipitation (MeRIP), followed by sequencing.

In the MeRIP sequencing analysis, peak density analysis indicated that Mettl14 deletion in DA neurons primarily decreased m6A peaks on the 3' UTR of RNA (Fig3.A). The sector graph displays the ratio of m6A peaks in each region of RNA (Fig3.B). Conditional knockout of Mettl14 in DA neurons resulted in a decrease in m6A levels in 6,366 genes, while an increase in m6A peaks was observed in 2,723 genes (Fig3.C). The chart displays the top three m6A consensus binding motifs with significant changes between Mettl14-cKO and control mice (Fig3.D). We further performed unbiased Gene ontology (GO) analysis for

the differential m6A-tagged transcripts. Notably, the most enriched biological processes were brain development, synaptic function, and GTPase activity (Supplementary Figure 5A). The heatmap reveals the top 30 genes with the most significant changes in m6A level on the transcripts in Mettl14-cKO mice compared to the controls (Supplementary Figure 5B).

The transcriptome sequencing data revealed that 227 genes were upregulated, while 374 genes were downregulated in Mettl14-cKO mice compared with control mice (Fig3.E). A heat map displayed the top 30 genes with the most significant changes in mRNA level (Fig3.F). GO analysis revealed that various biological functions were affected in Mettl14-cKO mice, including calcium ion homeostasis, actin cytoskeleton and transcription activator activity (Fig3.G).

These results suggest that the deletion of Mettl14 affects several critical biological functions of DA neurons, potentially underlying the mechanisms of Mettl14 deletion-induced DA neuron degeneration and impairment of dopaminergic function.

METTL14-mediated m6A modification impacts *Atp2a3* expression

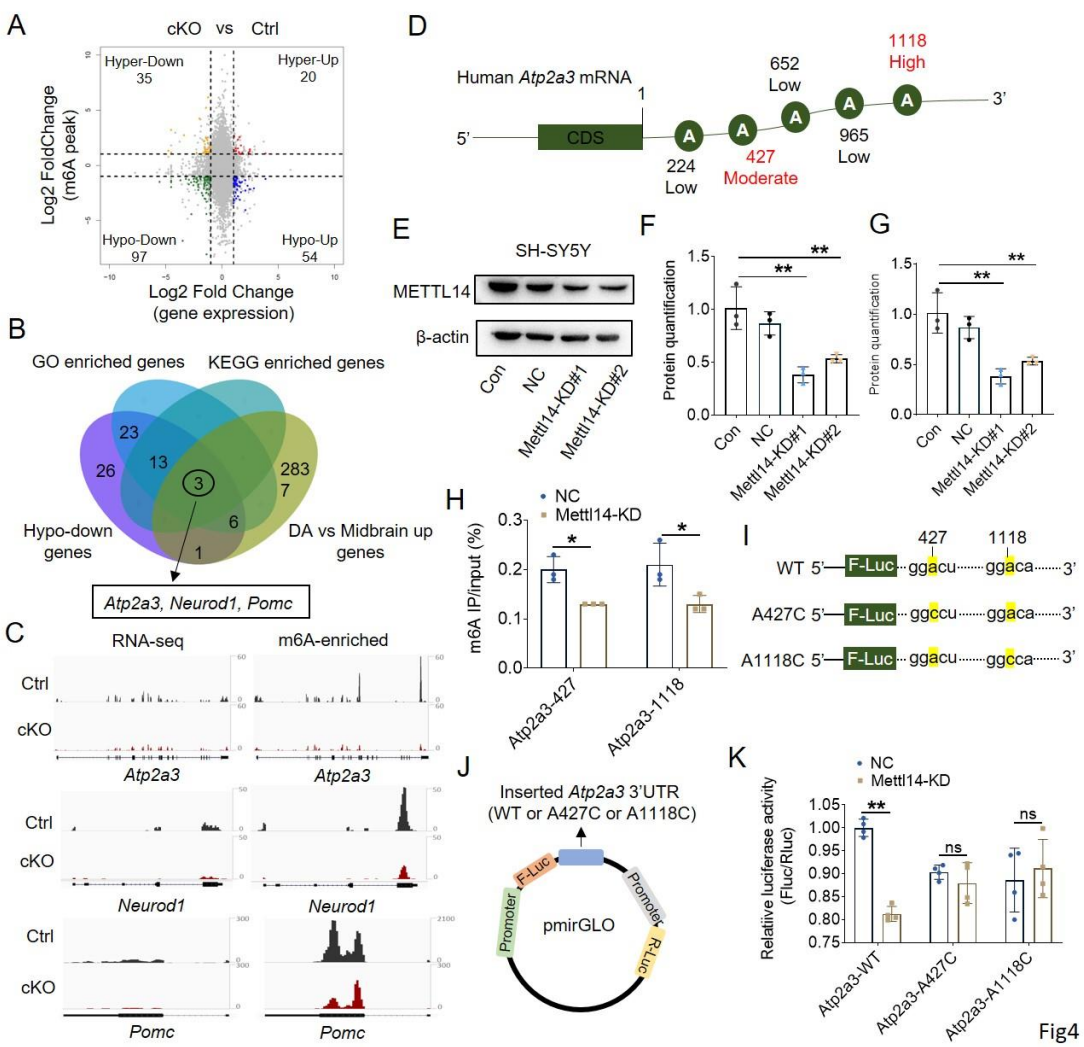

Fig4

To further

explore the underlying mechanism, we conducted an association analysis of the MeRIP-seq and RNA-seq data. The volcano plot depicted the intersection of the differentially genes based on the MeRIP-seq and RNA-seq data (Fig4.A). More than 200 genes with altered m6A methylation and differential expression were identified. Among the 151 hypomethylated genes, mRNA of 97 genes was downregulated (hypo-down), while 54 genes were upregulated (hypo-up) in Mettl14-cKO mice compared to the control. Heat maps listed the top 20 hypo-down (Supplementary Figure 6A-6B) and top 20 hypo-up genes (Supplementary Figure 6C-6D), which were ranked by mRNA expression level (Supplementary Figure 6A&6C) or m6A peak enrichment (Supplementary Figure 6B&6D), respectively. GO analysis revealed that hypo-down genes were mainly associated with functional units such as hormone secretion, walking behavior, and gene transcription activity (Supplementary Figure 6E), while hypo-up genes were mainly associated with functional unit of ion channel regulation (Supplementary Figure 6F). We further conducted a neural functional analysis of the hypo-down and hypo-up genes according to gene description and found that hypo-down genes are primarily related to neural development, metabolism, cytoskeleton, and transcriptional regulation, while hypo-up genes are mainly associated with ion channel activity, such as calcium, potassium channels (Supplementary Figure 6G). The differential genes that are highly related to each functional unit are displayed (Supplementary Figure 6H).

We next focused on hypo-down genes in the subsequent research, as genes exhibiting reduced transcription levels in Mettl14-cKO mice are more prominently affected according to transcriptome sequencing. We intersected genes enriched in both GO and KEGG analyses with genes known to be highly expressed in DA neurons[20], ultimately narrowing down to three genes of interest: ATPase sarcoplasmic/endoplasmic reticulum Ca^{2+} transporting 3 (*Atp2a3*), neuronal differentiation 1 (*Neurod1*), and Proopiomelanocortin (*Pomc*) (Fig4.B). The transcription and m6A modification levels of these three genes were significantly reduced, as indicated by both the transcriptome and MeRIP sequencing data (Fig4.C).

We focused on *Atp2a3* due to its crucial role as an intracellular pump located in the sarcoplasmic or endoplasmic reticulum (ER) of cells, mediating the translocation of calcium from the cytosol to the sarcoplasmic reticulum lumen. This function is vital for maintaining calcium homeostasis in the cytoplasm. Importantly, *Atp2a3* expression is significantly reduced in the brains of PD patients, making it a pertinent marker of PD[21]. Additionally, ATP2A3 serves as a molecular signature of dopaminergic neurons in the substantia nigra pars reticulate (SNpr), given its high expression in these neurons[22].

According to the SRAMP m6A site prediction website (http://www.cuilab.cn/sramp/), there are five m6A modification sites in the 3'UTR region of *Atp2a3* mRNA, confirming that *Atp2a3* can be regulated by m6A. The m6A site analysis revealed that site-1118 is a high m6A site, while site-427 is a moderate m6A site. The remaining sites (224, 652, 965) had lower scores (Fig4.D). Therefore, our subsequent mechanism study focused on site-1118 and site-427.

To confirm the regulatory effect of METTL14-mediated m6A modification on *Atp2a3* expression, we knocked downMettl14 in human neuroblastoma SH-SY5Y cells (Fig4.E&F). The RT-qPCR results showed

that the mRNA expression of *Atp2a3* in SH-SY5Y cells was decreased by half compared to the negative control (NC) after Mettl14 knockdown (Mettl14-KD) (Fig4.G), confirming the sequencing results. We then designed primers near site-427 and site-1118 to confirm the regulatory site of METTL14 at *Atp2a3* mRNA by using MeRIP assay. The results showed that the m6A level at both site-427 and site-1118 was decreased by approximately 40% (Fig4.H). This regulatory mechanism was further verified by the double luciferase reporter assay. The wild-type (WT) and mutated 3'UTR sequence of *Atp2a3* mRNA were inserted into the 3'UTR region of the reporter gene (Fig4.I-J). The results showed that in the WT *Atp2a3* mRNA group, Mettl14 knockdown attenuated the luciferin signal. However, the decrease in the luciferin signal by Mettl14 deficiency was reversed when the base "A" at site-427 or site-1118 was mutated into "C" (Fig4.K). Furthermore, the results indicated that within the NC group, in comparison to single-site mutations, the double mutation at site-427 and site-1118 could further decrease the luciferase activity (Supplementary Figure7), suggesting that the regulation of METTL14 on Atp2a3 might be multi-targeted.

Deficiency of Mettl14 disturbs calcium imbalance and triggers endoplasmic reticulum stress

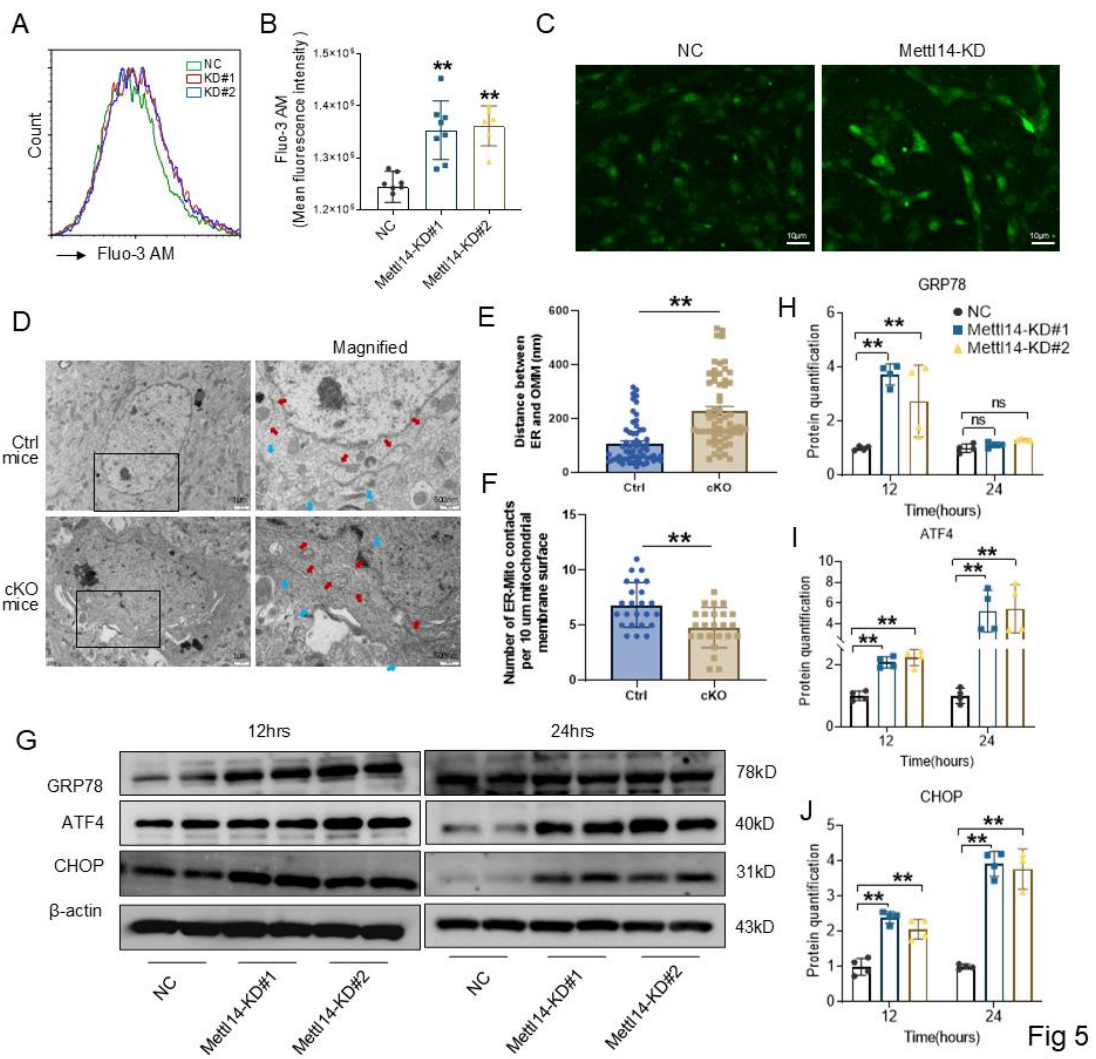

Fig 5

ATP2A3 is an important pump mediating the transfer of cytoplasmic calcium to the endoplasmic reticulum (ER), and its abnormal expression may lead to intracellular calcium imbalance. We used the Fluo-3 AM calcium indicator to detect the cellular calcium level and found that the calcium ions level in Mettl14 deficiency cells (Mettl14-KD) was significantly increased compared to control cells (NC)（Fig5.A-C）. Intracellular calcium imbalance may lead to damaged cellular homeostasis and excessive endoplasmic reticulum (ER) stress, we next detected the ER stress in Mettl14 deficiency neurons. Transmission electron microscopy showed typical morphology of excessive ER stress in the DA neuron in SN of Mettl14-KO mice, including extremely dilated or even fragmented ER (red arrow), damaged mitochondria with fragmented cristae (blue arrow in image) (Fig5.D). The Transmission electron microscope analysis demonstrated that, in comparison with the control mice, Mettl14-cKO mice exhibited a more pronounced expansion of the ER, increased distance between the ER and the mitochondria, and a diminished ER-mitochondria contact. This finding indicates that Mettl14-cKO results in impairment to ER-mitochondria contact, which may be a contributing factor to endoplasmic reticulum stress (Fig5.E-F). Moreover, examination of the unfolded protein response (UPR) signaling cascades in Mettl14-KD cells revealed activation of ER stress sensors, including glucose-regulated protein (GRP78 or BIP), and activating transcription factor 4 (ATF4), as well as increased protein levels of their downstream target genes proapoptotic transcription factor C/EBP-homologous protein (CHOP) (Fig5.G-J).

These results suggest that Mettl14 deficiency causes calcium ions imbalance and excessive ER disturbance, which may be the mechanism of Mettl14 deficiency-caused DA neuron loss.

Deficiency of Mettl14 renders cells susceptible to cell death

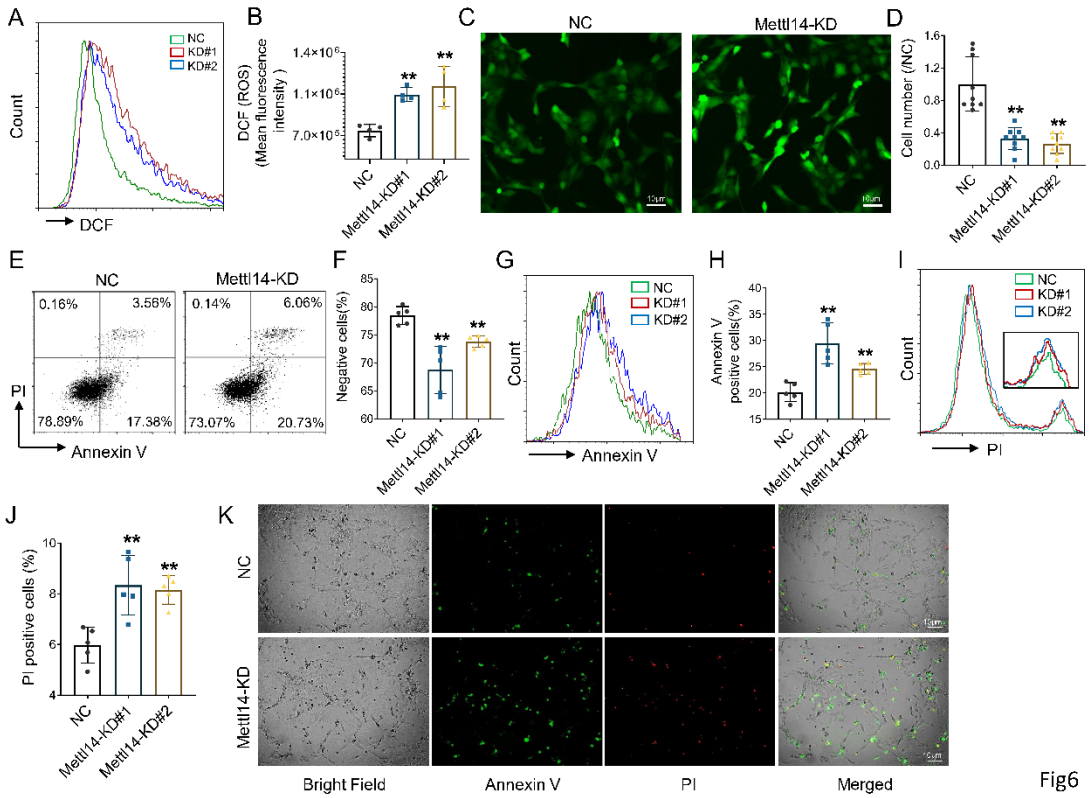

Fig6

Unresolved ER stress usually leads to oxidative stress and cell death by up-regulating proapoptotic proteins such as CHOP, we next further confirm whether loss of Mettl14 leads to increased oxidative stress and neuronal death. DCFH-DA does not fluoresce but can freely traverse the cell membrane. Once inside the cell, it is hydrolyzed by intracellular esterase into DCFH. Intracellular reactive oxygen species (ROS) can then oxidize non-fluorescent DCFH to produce fluorescent DCF (2',7'-dichlorodihydrofluorescein), with fluorescence intensity proportional to the ROS level. The mean DCF fluorescence intensity was quantified as a relative ROS level. Our findings indicated that, in comparison with the controls, the knockdown of Mettl14 led to a substantial increase in cellular ROS (Fig6.A-C) after 12 hours. Subsequently, there was a significant decrease in cell number after 24 hours (Fig6.D). Cell death was further measured by Annexin V and propidium iodide (PI) staining. According to the flow cytometry results, Mettl14 deficiency resulted in a decrease in the percentage of double Annexin V/PI-negative cells (Fig6.E-F), indicating reduced alive cells. Both Annexin V-positive cells (Fig6.G-H) and PI-positive cells (Fig6.I-J) were increased. The cells stained with Annexin V and PI were observed under a microscope, and similar results were obtained, the number of Annexin V-positive and PI-positive cells increased significantly in Mettl14 knockdown cells (Fig6.K).

Unexpectedly, we further observed a significant difference in the morphology of dead cells. Different from apoptotic features, the Mettl14 knockdown group exhibited bubble-like dead cells, similar to the phenotype of pyroptosis, which is mediated mainly by caspase 1/11 (Supplementary Figure 8A-8B). Therefore, we

next used apoptosis and pyroptosis inhibitors to treat cells and found that cell death triggered by Mettl14 knockdown could not be completely reversed by apoptosis inhibitor (caspase3 inhibitor), pyroptosis inhibitor (caspase1 inhibitor), or pan-caspase inhibitor (Supplementary Figure 8C). These results suggest that Mettl14 deficiency may cause complex unprogrammed cell death and that there may be other types of death other than apoptosis and pyroptosis. We indeed detected an approximate four-fold increase in the expression of ferroptosis marker gene (Acyl-CoA synthetase long-chain family member 4, *Acsl4*) and parthanatos marker gene (Apoptosis-inducing factor mitochondria-associated 1, *Aifm1*). Meanwhile, the expression of necroptosis marker gene (Mixed lineage kinase domain-like protein, *Mlkl*) was not changed (Supplementary Figure 8D).

These findings suggest that the loss of Mettl14 causes cells to be susceptible to cell death, and the pattern of death is complicated, possibly due to the disturbances in calcium homeostasis.

***Atp2a3* overexpression rescues ER stress and cell death in Mettl14-deficiency cells**

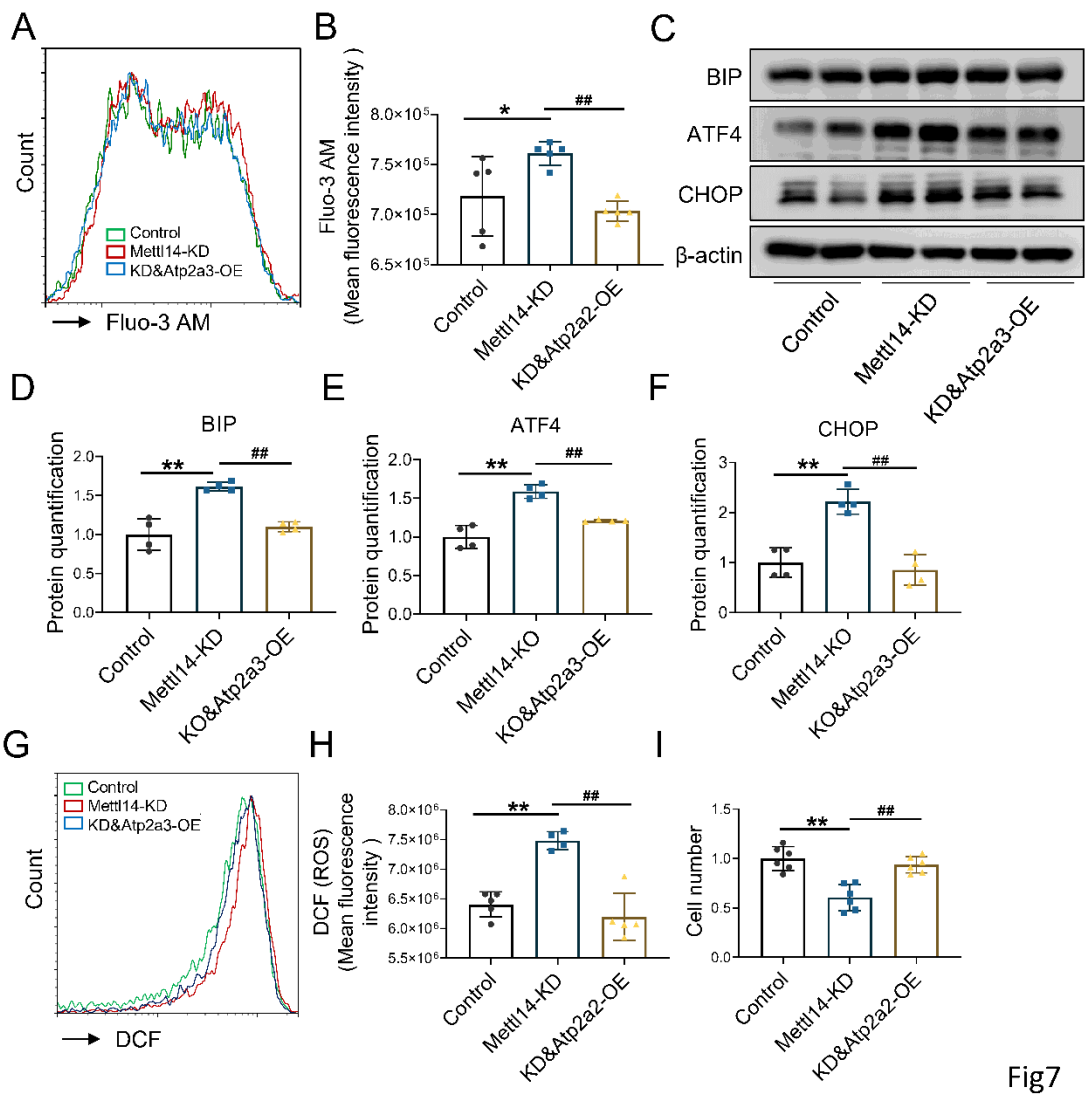

Fig7 To confirm

that *Atp2a3* is the key downstream mechanism of METTL14, we increased *Atp2a3* expression by exogenous plasmid (Atp2a3-OE) in Mettl14-KD cells and detected cellular calcium levels, ER stress sensors proteins expression, cellular ROS, and cell death. The results showed that Atp2a3-OE reversed Mettl14-KD-induced cellular calcium level increase (Fig7.A-B) and reduced the protein levels of GRP78, ATF4, and CHOP induced by Mettl14 deficiency (Fig7.C-F). Atp2a3-OE also rescued Mettl14 deficiency-induced cellular ROS accumulation (Fig7.G-H) and cell death (Fig7.I).

Together, these data further support our experiments in SH-SY5Y cells provide valuable insights into the role of METTL14 in regulating Atp2a3 mRNA and its impact on endoplasmic reticulum homeostasis, which could leads to neuronal loss as we observed in in vivo experiments.

Restoring Mettl14 alleviates PD-like phenotype in Mettl14-cKO mice

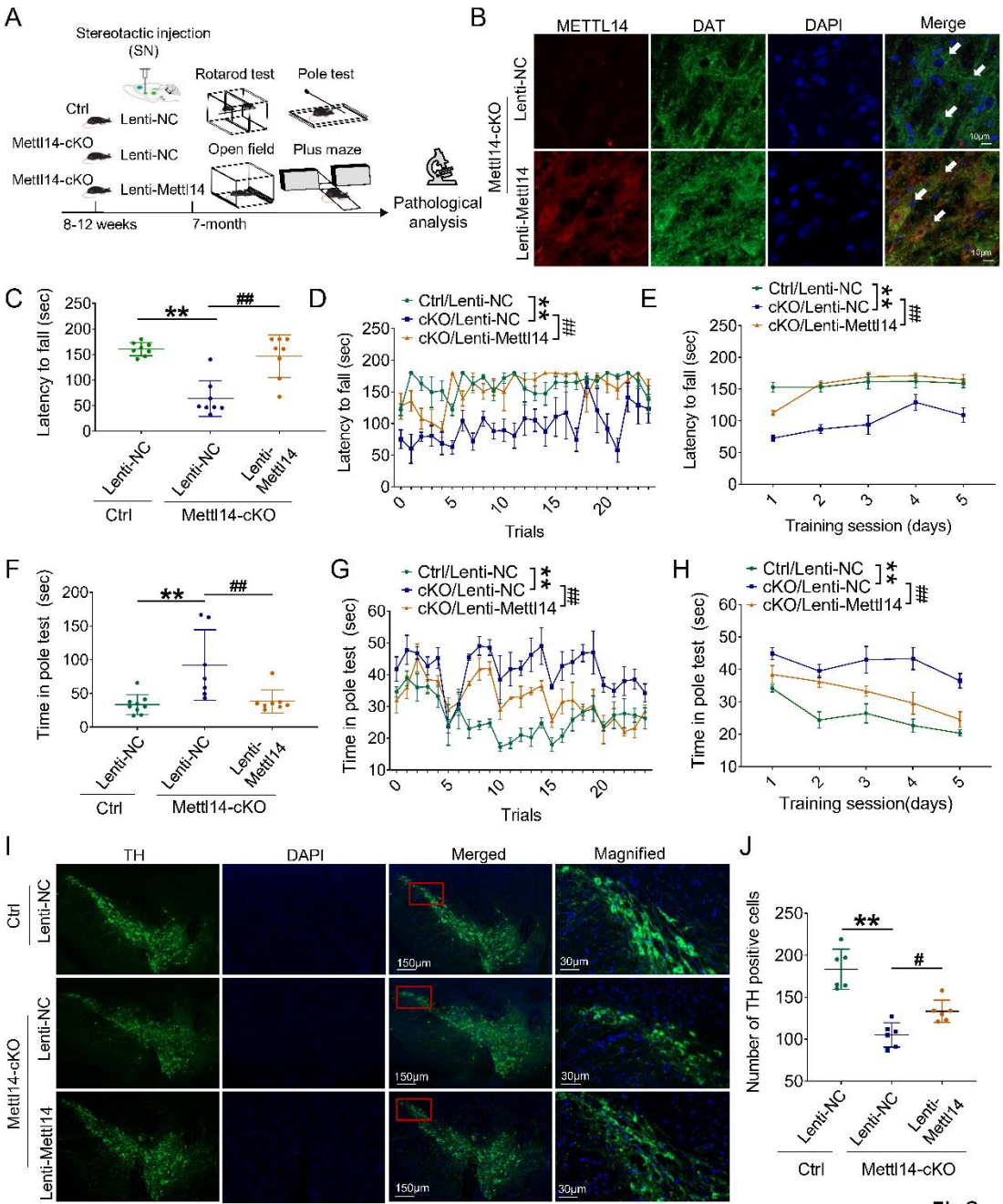

Fig8

We have demonstrated the importance of Mettl14 for DA neurons by vivo/in vitro experiments, finally, we would like to know if restoring expression of Mettl14 in SN region of Mettl14-cKO mice could improve the motor activities in these mice, which achieved by stereotactic injection of lentivirus containing the Mettl14 coding sequence (Lenti-Mettl14) (Fig8.A). Lentivirus absent Mettl14 coding sequence was used as the control (Lenti-NC). Immunofluorescence results indicated that the restoration of Mettl14 expression in DAT-positive cells of the SN region after Lenti-Mettl14 injection (Fig8. B). Rotarod and pole tests were conducted to show that restoring Mettl14 significantly improved the behavioral disorders caused by Mettl14

deletion (Fig8.C-H), although the pole test result showed that the cKO/Lenti-Mettl14 group mice need training to regain similar motor abilities as the Ctrl/Lenti-NC group (Fig8.G-H). However, there was no significant improvement in impaired locomotor activity induced by Mettl14 deletion, as determined by the open field (Supplementary Figure 9A-9C) and plus maze results (Supplementary Figure 9D-9F). Moreover, the number of TH positive cells in SN was increased in Lenti-Mettl14 group compared to Lenti-NC group in Mettl14-cKO mice, although it was not fully recovered to the level of Ctrl/Lenti-NC mice (Fig8. I-J).

Discussion

Our study has demonstrated the important role of METTL14 in the physiological function of DA neurons. Both Mettl14 mRNA and protein were reduced in SN of MPTP-treated mice and MPP^+-stimulated neurons. The conditional knockout of Mettl14 resulted in a decrease in dopamine neurotransmitter production and subsequent neuronal loss, ultimately impairing the locomotion ability of mice. MeRIP-Seq and mRNA-Seq revealed that Mettl14 deficiency led to significant changes in the gene expression profile in DA neurons, particularly in genes related to cell development and ion channels, including *Atp2a3*, a potential marker for PD diagnose. The deletion of Mettl14 led to a decrease in Atp2a3 expression by reducing the m6A modification on the 3'UTR of its mRNA. It is likely that this involves multi-target regulation rather than single-target regulation. This situation resulted in an imbalance of calcium between the endoplasmic reticulum (ER) and cytoplasm, as well as ER stress, ultimately leading to cell death. Further studies indicated that lentivirus-mediated restoration of Mettl14 expression in Mettl14-cKO mice relieved the impaired motor activities, indicating the clinical relevance of m6A dysregulation to DA neuron-mediated behavioral changes. Modulation of the m6A level may have therapeutic potential for treating PD.

The dynamic regulation of m6A in the adult brain is an important epitranscriptomic mechanism associated with brain function and behavioral adaptation[9,23-29]. METTL14-mediated m6A modification has been reported to be involved in neurogenesis and brain function. Mettl14 deletion significantly reduces the proliferation and early differentiation of embryonic neural stem cells, resulting in a reduction in the number of late-born neurons [30]. Mettl14 knockout in the embryonic mouse brain prolongs the cell cycle of radial glia and cortical neurogenesis [31]. Inhibition of METTL14 attenuates sciatic nerve lesion-induced overall protein translation in the dorsal root ganglion of adult mice, thereby reducing axonal regeneration in the peripheral nervous system[4]. METTL14 is also essential for oligodendrocyte maturation and central nervous system (CNS) myelination. Inactivation of METTL14 in oligodendrocytes results in decreased oligodendrocyte numbers and hypomyelination in the CNS[32]. METTL14 has been shown to play an important role in maintaining normal striatal function in adult mice. Conditional knockout of Mettl14 in the striatum severely impairs striatal-mediated behavioral phenotypes[33]. These results indicate that METTL14 is essential for the function of a wide range of brain cells, including neural stem cells, glial cells, and neurons. Previously, we reported that lentivirus-mediated conditional Mettl14 deficits in the substantia nigra could affect dopaminergic neuron-mediated behavioral functions[11]. By using the LoxP-Cre system, we generate DA neuron-specific Mettl14 knockout mice and elucidate the effects of METTL14 on DA neurons. Results

from the current study are consistent with our previous findings that the loss of Mettl14 in DA neurons leads to impaired motor activities, which may be relevant to the gradual loss of DA neurons in the SN region followed by disturbed nigrostriatal dopamine system. Our results confirm that METTL14 is essential for DA neurons- regulated behavioral functions and further illuminate the underlying regulatory mechanism of METTL14-mediated m6A modification on DA neurons in the brain. Regarding the anxiety phenotype observed in Mettl14 cKO mice based on the open field and elevated plus maze tests, we are also intrigued by this finding. These results are not necessarily indicative of impaired motor function, We hypothesize that this anxiety-like behavior may not be directly linked to the SN DA neurons but could be related to broader neural circuit changes or inflammation caused by neuronal damage. It's also possible that the anxiety phenotype stems from a different DA neural circuit affected by Mettl14 cKO. We are planning to investigate this in future studies using this mouse model.

Based on our sequencing data, the Mettl14 deficiency induced-hypo-down genes appear to play a crucial role in brain development and cell protection. Further analysis revealed that ATP2A3, a member of the sarco-endoplasmic reticulum calcium ATPase (SERCA) pump family, which includes SERCA1, SERCA2, and SERCA3 (or ATP2A1-3 in humans), may be a key molecular mechanism underlying dopaminergic neuronal dysfunction after Mettl14 deletion. SERCA family including ATP2A3 regulates intracellular Ca^{2+} homeostasis by transporting calcium from the cytosol to the lumen of the sarco-endoplasmic reticulum[34]. Our findings validate the role of Mettl14 in maintaining calcium ion homeostasis. The deletion of Mettl14 results in an elevation of cytoplasmic calcium levels. Nevertheless, Fluo3-AM, being a calcium sensor, does not enable us to ascertain whether the calcium originates from the ER, mitochondria, or cytosol. Recent research has implicated ATP2A3 in Parkinson's disease, where it is enriched in dopaminergic neurons in the substantia nigra region and serves as a molecular marker of these neurons[22]. A sequencing analysis of brain tissue from PD patients demonstrated that *Atp2a3* mRNA levels were significantly reduced compared to healthy controls, suggesting that ATP2A3 may serve as a potential biomarker and molecular target for PD[21]. In fact, studies have reported that the treatment of SERCA activators has a role in alleviating motor disorders caused by 6-OHDA injury in rats [35].

Under several physiological or pathological conditions, such as calcium ion disorder, failure of proteins to form normal disulfide bonds, or changes in redox status, unfolded or misfolded proteins aggregate in the ER and disrupt its normal physiological function. This process is called ER stress. ER stress is followed by an adaptive response via the activation of the unfolded protein response (UPR), involving pathways such as PERK, inositol-requiring transmembrane kinase/endoribonuclease 1α (IRE1α), and activating transcription factor 6 (ATF6), to re-establish intracellular environmental homeostasis. However, ER stress can be a double-edged sword. Excessive ER stress activates the PERK/eukaryotic initiation factor 2α (eIF2α) signaling pathway, leading to the translocation of ATF4 into the nucleus where it interacts with CHOP. Subsequently, the expression of apoptosis-related genes is promoted, inducing an oxidative stress response and cell death [36,37].

Accumulating evidence supports the role of ER stress as a principal player in dopaminergic neurons cell death. In human brain tissues, ER stress markers, such as phosphorylated PERK and phosphorylated eIF2α, were detected in neuromelanin containing dopaminergic neurons of the substantia nigra of PD patients but

not in control cases. Activation of UPR has also been observed in various animal or cell models of PD[36,37]. More importantly, SERCA family have been shown to be dysregulated in animal model of PD, resulting in calcium balance disorder-induced ER stress and oxidative stress, ultimately contributing to neuronal death and driving PD pathogenesis[35]. Combined with the decreased expression of *Atp2a3* in the brains of PD patients, it is suggested that the decrease in *Atp2a3* levels may be the molecular mechanism inducing calcium ion disorder, ER stress, and neuronal death in DA neurons of PD patients.

In recent years, studies have shown that m6A related proteins are associated with ER stress in cells. Deficiency of the m6A writer METTL3 enhances the expression and stability of the YTH N6-methyladenosine RNA binding protein F2 (YTHDF2)-mediated *Grp78* mRNA, upregulating the expression of ER stress-related proteins and inducing osteoblast apoptosis[38]. METTL3 potentiates progression of cervical cancer by suppressing ER stress via regulating m6A modification of thioredoxin domain containing protein 5 (*Txndc5*) mRNA, which is a protein disulfide isomerase located in the ER[39]. METTL3 is reported to have a harmful effect on a preeclamptic rat/cell model under ER stress as it decreases the levels of transmembrane BAX inhibitor motif containing 6 (*Tmbim6*) mRNA[40]. METTL14 can directly promotes *Chop* mRNA decay through its 3'UTR m6A modification, thereby inhibiting the expression of downstream proapoptotic target genes. When stimulated by toxin, Mettl14 deficiency makes the liver more susceptible to ER stress and liver damage[41]. Loss of Mettl14, but not of Mettl3, results in the hypomethylation of mRNA transcripts involved in the ER stress response, leading to unresolved ER stress and hepatocyte death [42]. In triple-negative breast cancer, METTL14-modificated ubiquitin-specific protease 19 (USP19) increases the level of ER calcium by regulating the stability of chaperone regulator 6 (BAG6) and B-cell lymphoma 2 (BCL2) protein. This leads to ER stress and tumor cell death[43]. Another m6A writer, Wilms' tumor 1-associating protein (WTAP), can promote myocardial ischemia/reperfusion injury by increasing ER stress via regulating m6A modification of *Atf4* mRNA[44]. m6A eraser AlkB Homolog 5 (ALKBH5) serves an important role in maintaining ER homeostasis and cellular fitness. ALKBH5 regulates ER homeostasis by controlling the expression of ER lipid raft associated 1 (ERLIN1) to maintain the calcium flux between the ER and mitochondria[45]. In stroke, *Alkbh5* knockdown can aggravate ER stress, neuroinflammation and neuronal apoptosis by promoting the stability and expression of *Stat5* mRNA[46]. Additionally, loss of m6A reader YTH N6-methyladenosine RNA binding protein F1 (YTHDF1) inhibits the activation of signaling pathways associated with ER stress, thereby inhibiting the differentiation and function of inflammatory osteoclasts[47].

However, whether m6A is involved in regulating ER stress in DA neurons of PD has not been reported. Only an *in vitro* study has shown that reducing m6A levels through FTO overexpression or m6A inhibitors can induce apoptosis in DA neurons by increasing oxidative stress and Ca^{2+} influx[12].In the present study, we first demonstrated METTL14 is essential for cellular homeostasis in DA neuron. Reduction in METTL14-mediated changes in *Atp2a3* expression leads to calcium disorder and ER stress in DA neurons, ultimately resulting in cellular dysfunction and cell death.

Our *in vitro* study has demonstrated that deficiency of Mettl14 causes cellular death of SH-SY5Y cells. Thus, we were unable to construct Mettl14-knockout cell lines. Further investigation revealed that this process is not solely cell apoptosis, as a caspase-3 inhibitor cannot completely reverse the phenomenon. We observed that Mettl14-deficient cells exhibited a bubble-like phenotype, indicating changes in cell membrane permeability, which may be indicative of pyroptosis [48]. Pyroptosis is caused by caspase1-mediated gasdermin D (GSDMD) activation, leading to the formation of pores in the cell membrane and changes in cell permeability[49]. However, neither caspase-1 nor pan-caspase inhibitors could completely reverse Mettl14 depletion mediated cell death, indicating that there may be other types of cell death.

It is known that neurons can undergo various forms of cell death, with currently more than ten known types identified[50]. Our study has also shown that the marker genes associated with parthanatos and ferroptosis were significantly increased in Mettl14-deficient SH-SY5Y cells, indicating that METTL14 inactivation may also induce ferroptosis and parthanatos in neurons. According to the sequencing data, the expression of solute carrier family 40 member 1 (Slc40a1, also known as Fpn1) is also altered upon Mettl14 depletion in DA neurons. Interestingly, SLC40A1 is the only discovered mammalian iron efflux transporter in the plasma membrane and mediates iron release from cells. Studies have indicated that Slc40a1 dysregulation results in the intracellular iron overload and lipid peroxidation, thereby inducing ferroptotic cell death [51,52], which is correlated with the ferroptosis marker we detected in the Mettl14-deficient SH-SY5Y cells in our study.

It is worth mentioning that the results we obtained from conditional knockout mice differed somewhat from those detected in Mettl14-deficient SH-SY5Y cells. Mettl14 deletion in cells directly leads to disordered cell death. However, in aged conditional Mettl14 knockout mice, we still observed a significant number of DA neurons in the substantia nigra region. This difference reflects the complexity and significance of m6A modification in vivo. Since this post-transcriptional modification can be achieved by a methyltransferase complex including METTL3/14, WTAP and several supporting proteins, embryonic depletion of Mettl14 in cKO mice may trigger the supplementary machinery to regulate m6A in DA neurons. While aging is often associated with a loss of function, the temporary balance of m6A modification in young cKO mice might be disrupted upon aging. As dopaminergic function declines with normal aging and increased inflammatory burden, altered expressional profile lead to the current imbalances, including calcium, potassium, sodium, iron, as well as neurotransmitters. These imbalances ultimately lead to the loss of DA neurons and impaired motor activities in aged cKO mice.

In summary, our study underscores the pivotal role of METTL14 in maintaining the physiological function of DA neurons. We demonstrated that METTL14 deficiency leads to reduced Atp2a3 expression through decreased m6A modification on its mRNA 3'UTR, resulting in ER/cytoplasm calcium imbalance, ER stress, and subsequent neuronal death. These efforts will enhance our understanding of the complex interplay between m6A regulation, ER homeostasis, and neuronal survival, potentially paving the way for novel therapeutic strategies.

Methods

Chemical reagents and antibodies

MPTP (1-Methyl-4-phenyl-1,2,3,6-tetrahydropyridine) and MPP^+(1-methyl-4-phenylpyridine) were purchased from Sigma-Aldrich (M0896; D048). Caspase1 inhibitor (Z-YVAD-FMK, S8507), caspase3 inhibitor (Z-DEVD-FM, S7312) and pan-caspase inhibitor (Z-VAD-FMK, S7023) were the product of Selleck Chemicals. Anti-m6A primary antibody (ABE572) was from Millipore. Anti-TH (25859-1-AP), DAT (22524-1-AP) and β-actin (60008-1-Ig) primary antibodies were purchased from Proteintech Group. Anti- METTL14 (ab220030) and ATF4 (ab23760) primary antibodies were from Abcam. Anti-pPERK(SC-32599), PERK(SC-13073), GRP78(SC-33757), CHOP (SC-7351), PITX3(SC-19307) and NURR1 (SC-81345) primary antibodies were from Santa Cruz Biotechnology. Anti-mouse IgG (7076P2) and anti-rabbit IgG (7074P2) secondary antibodies were from Cell Signaling Technology (CST). Alexa fluor 594-conjugated goat anti-rabbit IgG (H+L) cross-adsorbed secondary antibody (A11012), Alexa fluor 488-conjugated goat anti-rabbit IgG (H+L) cross-adsorbed secondary antibody (A11008), Alexa fluor 594-conjugated goat anti-mouse IgG (H+L) cross-adsorbed secondary antibody (A11005) and Alexa fluor 488-conjugated goat anti-mouse IgG (H+L) cross-adsorbed secondary antibody (A11001) were from Thermo Fisher Scientific. Cell membrane permeable calcium fluorescent probe Fluo-3 AM (40703ES50) was purchased from Yeasen Biotechnology. DCFH-DA (2′,7′-dichlorodihydrofluorescein diacetate, CA1410) for reactive oxygen species detection was obtained from Solarbio life Sciences.

Animals

All animal procedures in this study were approved by the Institutional Animal Care and Use Committee of Sichuan Provincial People's Hospital. C57BL/6 background Mettl14-loxp ($Mettl14^{(f/f)}$) mice were generated by CRISPR/Cas9-based genome editing technology[11]. C57BL/6 background DAT-cre was from Jackson lab ($Slc6a3^{tm1.1(cre)Bkmn}$). Conditional dopaminergic neuron Mettl14 knockout mice were constructed by crossing Mettl14-loxp mice with DAT-cre mice. The genotypes of homozygote and heterozygote were identified by PCR and agar gel electrophoresis. The experiments were conducted using a total of 9 mice in each group, with an equal number of male and female mice to ensure balanced representation across all groups. All mice were housed in a standard environment with 12-hour light/dark cycle and had access to food and water at a temperature of 22 ±1℃.

Viral injection

8-12-week-old mice were anesthetized using 2% isofluorane. Mice were then injected with a lentivirus (10^8 TU/mL, GenePharma) into the substantia nigra region (AP: -3.4 mm, ML: ±1.5 mm, DV: -4.5 mm) under sterile conditions.A total of 2μL of lentivirus with Mettl14 mRNA (Lenti-Mettl14) or empty ctrl (Lenti-NC) was delivered at a rate of 0.5μL per minute. The virus was allowed to diffuse for eight minutes after injection, followed by needle extraction.

Behavioral test

The rotarod test was conducted using a computer-controlled rotarod apparatus (SA102, SANS) with a rod of 7 cm in diameter, the rotary speed was set to accelerate from 0 to 40 revolutions per minute (rpm) over 300 seconds and each mouse is recorded for 5 minutes. . The time to fall (latency to fall) was recorded. At nine months of age, mice were subjected to five consecutive trials per session. There was one session per day for a total of five days, with intertrial intervals of approximately 30 seconds. The pole test consists of a platform with a 40-cm length pole, where the rod is positioned at a 90-degree angle to the platform. Mice were placed at either the bottom or top of the pole, and the time taken to climb from bottom to top (t1) or descend from top to bottom (t2) was recorded. The sum of t1 and t2 was calculated as the total time in the pole test. Mice aged between 3 and 11 months belong to the same cohort. Nevertheless, owing to the sacrifice of some mice during this period for the purpose of obtaining brain tissues for detection, the number of 11 - month - old mice has decreased. The data of 1 - month - old mice are derived from a new cohort.

An open field chamber with tetrahedral walls measuring 40 × 40 cm in diameter was divided into two parts: the periphery and the center zone. The motion track of mice was recorded by infrared beams using a computer-connected camera. Data were collected for five minutes per mouse, and the time, total distance, and entries in the center zone were calculated. The elevated plus maze consists of an open arm (40-cm length) and a closed arm (with walls, 40-cm length). Mice were placed in the center of the plus maze, and their motion track was recorded using the same method as in the open field. Data were collected for five minutes per mouse, and the time and total distance in the open arm, as well as the resting time in the closed arm, were calculated.

Primary neuron isolation

Primary neurons were obtained from fetus of ICR (Institute of Cancer Researcch) mice at 16-17 days of pregnancy, which were purchased from Chengdu Dossy experimental animals' company. All animal procedures were performed according to the protocols approved by the Institutional Animal Care and Use Committee of Sichuan Provincial People's Hospital. 24-well or 6-well plate were pre-coated with Poly-L-ornithine solution for at least two hours, and then washed with sterilized ddH2O twice. The brain cortex was dissected in iced HBSS, and digested by trypsin-EDTA (Gibco,25200-056) with DNAase (Solarbio,310D031). Cells were then pelleted by centrifugation and resuspended in DMEM/F12 medium supplemented with 10% FBS (fetal bovine serum, ZETA, Z7186FBS-500),1×GlutaMAXTM-I (Gibco,35050-061), 1% Penicillin-Streptomycin antibiotics (Solarbio, P1400) and 0.5% glucose. Cells were then planted in Poly-L-ornithine coated plates and culture at 37℃ in a 5% CO_2 incubator for 4-6 hours. The culture medium was changed to Neurobasal medium (Gibco, 21103-049) with 10% FBS,1×GlutaMAXTM-I, 1×B27 supplement (Gibco,17504-044) and 1% Penicillin-Streptomycin antibiotics, and sequentially culture for 4-7 days.

Cell culture and treatment

Human neuroblastoma SH-SY5Y cell line was cultured in MEM/F12 medium supplemented with 10% FBS and 1% Penicillin-Streptomycin antibiotics at 37℃ in a 5% CO2 incubator. SH-SY5Y cells or primary

neuron were treated with different concentration of MPP^+, caspase 1 inhibitor (Z-YVAD-FMK), caspase3 inhibitor (Z-DEVD-FM) and pan-caspase inhibitor (Z-VAD-FMK as indicated time before detection.

Dot blot

Total RNA from substantia nigra region was obtained the same as RT-qPCR. 100ng and 200ng RNA in 2μL volume was dropped on a nitrocellulose membrane. Membrane was then crosslinked by ultraviolet exposure (Ultraviolet Crosslinker, Analytik jena), followed by blocking with 5% non-fat milk diluted in TBST for one hour at room temperature. Anti-m6A primary antibody (1:1000) was added and incubated with membrane at 4℃ overnight. The next day, m6A antibody was removed by washing with TBST and membrane was incubated with secondary antibody for one hours at room temperature. The RNA was detected by an HRP chemiluminescence kit under the Tanon-5200 chemiluminescence imaging analysis system. Quantification of the blots was assessed by Image J.

Immunofluorescence

Mice were perfused with a 1×PBS solution and 4% paraformaldehyde solution after euthanasia. The brain was anatomically removed and soaked in a 4% paraformaldehyde solution for 24 hours. Subsequently, the brain was transferred to a 30% sucrose solution, and the solution was changed every 24 hours until the brain sank to the bottom. Coronal brain sections with a thickness of 30 μm were obtained using a freezing microtome (CM1860, Leica Instruments). The brain sections were soaked in a 0.3% TritonX-100 solution for 20 minutes and blocked with 10% goat serum for 20 minutes. Following this, the brain sections were incubated with TH, METTL14, or DAT antibodies (1:200) overnight at 4 ℃. The next day, the brain sections were washed and incubated with a fluorescence-conjugated secondary antibody for one hour at room temperature. Finally, the sections were counterstained with DAPI and immersed in mounting medium before being sealed on a slide with nail polish. Images were captured using a confocal microscope (LSM800, ZEISS).

Immunohistochemistry and stereology

For histological analysis, Brain tissues were isolated and dissected. One hemisphere was submitted for sectioning and staining. Prior to immunostaining, sections were subjected to protein blocking using 5% bovine serum albumin (BSA) supplemented with 0.1% Triton X-100 in PBS for sixty minutes at room temperature to minimize nonspecific interactions. Primary antibody targeting tyrosine hydroxylase (1:3000) was applied overnight under controlled humidity. Secondary detection utilized horseradish peroxidase-conjugated IgG fractions (1:200 dilution) with a 60-minute incubation period. Chromogenic visualization was accomplished through diaminobenzidine tetrahydrochloride (DAB) substrate development according to manufacturer protocols. Sections were cut at 60 μM, stained with anti-tyrosine hydroxylase antibodies, and then counterstained with Nissl. Quantitative assessment of dopaminergic neurons in the substantia nigra (SN) was performed using stereological principles with Visiopharm Phenolex software (Denmark), applying systematic random sampling for unbiased cell counting, counting every fourth section of the SN region (5 sections/animal).

Dopamine (DA) transmitter examination

The fresh tissue of the substantia nigra was separated, and total protein was extracted. The total concentration of the extracted protein sample was diluted to 300 ng/μL, and the dopamine (DA) level in the substantia nigra was measured by enzyme-linked immunosorbent assay (ELISA) according to the manual provided by the manufacturer (EM1712, Fine Biotech).

Golgi staining

Golgi staining was performed using the FD Rapid GolgiStain dye kit according to the manufacturer's manual (PK401, FD NeuroTechnologies). After euthanasia, the mouse brain was quickly removed from the skull. The fresh mouse brain was soaked in A/B mixed solution, which was replaced with a new A/B mixed solution after 12-18 hours, and then left in the dark for 15 days. The mouse brain was then transferred to solution C, which was replaced with a new solution C after 24 hours, and left in the dark for 72 hours. Coronal brain sections with a thickness of 100 μm containing the substantia nigra pars compacta (SNpc) were prepared using a freezing microtome and mounted on gelatin-coated microscope slides. The brain sections were then stained and dehydrated following the manufacturer's instructions. Image scanning was performed using Pannoramic MIDI (3DHISTECH).

Methylated RNA Immunoprecipitation (MeRIP) and mRNA-sequencing

MeRIP/mRNA-sequencing projects and subsequent data analysis were supported by Genesky Biotechnologies Inc. (Shanghai, China). One-year-old Mettl14-cKO and Ctrl mice were perfused with 1×PBS solution after euthanasia. The substantia nigra tissue was quickly dissected, and total RNA was extracted using TRIZOL reagent (15596-026, Invitrogen). Total RNA from three mice for each group was combined into one sample. Subsequently, the mixed RNA samples were precipitated by an m6A antibody and subjected to sequencing.

Plasmid Constructs

The sgRNAs (gRNA#1: AGA TAC TTA CGT TTT GCA TT, gRNA#1: ACG TTT TGC ATT TGG AGC AG) specifically targeting Mettl14 were designed based on recommendations from the Zhang laboratory website (http://crispr.mit.edu/). To construct the gRNA expression plasmid, complementary oligonucleotides encoding gRNAs were annealed and cloned into BsmBI (Fermentas) sites in lentiCRISPRv2 (Addgene). The Mettl14 knockdown (Mettl14-KD) SH-SY5Y cell line was generated by transfecting the lentiCRISPRv2-gRNA plasmid using Lipofectamine 2000 reagent (11668019, Invitrogen) and Opti-MEM (31985062, Gibco) according to the manufacturer's instructions. An empty lentiCRISPRv2 plasmid was used as a negative control (NC). Western blotting was performed to detect the effect of gRNA knockout 48 hours after transfection.

The full length of the human *Atp2a3* 3′ UTR regions, including the wild type, 427-site mutation (A to C), and 1118-site mutation (A to C), were cloned into the pmirGLO luciferase reporter plasmid (Promega) via PmeI and NheI restriction sites. For experimental validation of *Atp2a3* 3′ UTR as a target of METTL14, co-transfections of reporter constructs and lentiCRISPRv2-gRNA plasmid were carried out in SH-SY5Y

cells. After 24 hours of transfection, cells were lysed, and luciferase activity was measured on 96-well black plates in a Microplate reader (Varioskan Lux, Thermo Fisher Scientific). Luciferase activities were measured as the relative activity of firefly/Renilla luciferase (F-luc/R-luc) using a Double-Luciferase Reporter Assay Kit (FR201-01, TransGen Biotech).

Cell death detection

SH-SY5Y cells were cultured in a 24-well plate and transfected with plasmids. After 24-48 hours, the total cell number was counted. Dead cells were detected by Annexin V-FITC and propidium iodide (PI) staining using an Annexin V Detection Kit (BD Biosciences) following the manufacturer's protocol. The death of cells was assessed by flow cytometry (NovoCyte Quanteon, Agilent Technologies). Cells that were negative for both Annexin V and PI were defined as healthy cells. The morphology of cells was recorded by microscopy.

Western blot (WB) assay

SH-SY5Y cells or brain tissues were lysed in RIPA buffer (R0010, Solarbio) supplemented with protease inhibitor and phosphatase inhibitor (04693132001 and 04906837001, Roche). The protein concentration was quantified using a BCA kit (CA1210, Solarbio). Protein samples were mixed with loading buffer and then boiled at 98°C for 5 minutes. Equal amounts of protein samples were electrophoresed in a sodium dodecyl sulfate-polyacrylamide gel (10%–12.5%) followed by transferring to PVDF membranes (Millipore). PVDF membranes were blocked with 5% non-fat milk (232100, BD Biosciences) for one hour at room temperature, and the blots were probed with primary antibodies and secondary antibodies. The blots were finally detected using an HRP chemiluminescence kit (WBKLS0100, Millipore) under a chemiluminescence imaging analysis system (5200, Tanon). Quantification of the blots was assessed using Image J. Protein expression is normalized to β-actin, the quantitative data represent the relative values compared to the control group.

Real-time quantitative polymerase chain reaction (RT-qPCR)

Total RNA was extracted using TRIZOL Reagent (15596-026, Invitrogen), and cDNA was synthesized (R323-01, Vazyme) following the manufacturer's instructions. The synthesized cDNA was then amplified and detected using Syber green PCR mixture (Q711-02/03, Vazyme), a real-time fluorescence quantitative PCR instrument (ABI7500, Thermo Fisher Scientific), and the following primers: human Atp2a3(forward: 5'- CAC GGA GAC AGC TCT GAC TTG C -3', reverse: 5'- ACA TGG ATT TCC GGT CTC GGG A -3'), human Mettl14(forward: 5'- AGA AAC TTG CAG GGC TTC CT -3', reverse: 5'- TCT TCT TCA TAT GGC AAA TTT TCT T-3'), mouse Mettl14(forward: 5'-GAG CTG AGA GTG CGG ATA GC -3', reverse: 5'- GCA GAT GTA TCA TAG GAA GCC C-3'), human Acsl4(forward: 5'- CAT CCC TGG AGC AGA TAC TCT-3', reverse: 5'- TCA CTT AGG ATT TCC CTG GTC C -3'), human Aifm1(forward: 5'- TTC CAG CGA TGG CAT GTT CC-3', reverse: 5'- TCC TAC TGT TGA TAA GCC CAC A -3') , human Gapdh primers (forward: 5'- TGC ACC ACC AAC TGC TTA GC -3', reverse: 5'- GGC ATG GAC TGT GGT CAT GAG -3') and mouse Gapdh primers (forward: 5'- CTACACTGAGGACCAGGTTGTC -3',

reverse: 5'- GTTATTATGGGGGTCTGGGATGG-3').

Methylated RNA Immunoprecipitation (MeRIP)

The m6A level of Atp2a3 mRNA in control and Mettl14-KO SH-SY5Y cells was measured using the MeRIP m6A kit (17-10499, Millipore). All operations were carried out according to the instruction manual provided by the manufacturer. Twenty-four hours after gRNA transfection, total RNA was extracted using TRIZOL Reagent and fragmented using fragmentation buffer. m6A-modified RNA was precipitated by magnetic beads and anti-m6A antibody. Finally, the m6A level was detected by one-step PCR. Normalized $\Delta Ct=Ct$ (IP m6A) - (Ct(input)-$\log_2$[10]), %input=$2^{(-\text{Normalized } \Delta Ct)}$. Detection primer forward, 5'-GTT CAC TTG GTG ACT GGT GCC-3' and reverse, 5'-GAG GTC AGA GCC GGT AAG AAG G-3' for the site 427 of *Atp2a3* mRNA. forword, 5'- GGA AGA TGG CCT CTG ATG GAC A -3' and reverse, 5'- CCC CTC GCT AGT TTT TGC CAA A -3' for the site 1118 of *Atp2a3* mRNA.

Transmission electron microscope analysis of the ER

One-year-old Mettl14-cKO and Ctrl mice were perfused with 1×PBS solution after euthanasia. The substantia nigra tissue was quickly dissected. Brain samples were prefixed with 3% glutaraldehyde and then fixed with 1% osmium tetroxide. After step-by-step dehydration with acetone, samples were coated with Epon-812 agent. The areas enriched with neurons of the brain sample were selected by the semi-thin section under the light microscope, and the 60-90nm ultra-thin section was made by the ultra-thin microtome and the sections were put in the copper grid. Dye the sections with uranyl acetate for 10~15min, followed by lead citrate for 1~2min. Finally, the endoplasmic reticulum and mitochondria of neurons were observed under a transmission electron microscope (JEM-1400FLASH, JEOL, Japan).

Statistical analysis

All data were analyzed using the two-tailed unpaired Student's t-tests between two groups. One-way or two-way analysis of variances (ANOVA) were used for multiple comparisons. All data were graphed, and statistical analyses were performed using Prism 8 (GraphPad Software), significance was defined as $P < 0.05$. The number of sections, cells, and mice used in each experimental group were indicated in legends.

Availability of data and materials

The datasets generated and analyzed during the current study are not publicly available due to privacy, but are available from the corresponding author upon reasonable request.

Acknowledgments

The authors would like to thank Dr. Li Hua-bing (Shanghai Institute of Immunology, State Key Laboratory of Oncogenes and Related Genes, School of Medicine, Shanghai Jiao Tong University) for his support to provide us the Mettl14-loxp mice. L.Y. and W.D.L discloses support for the research of this work from the National Natural Science Foundation of China (81601125, 32220103006) and the Department of Science and Technology of Sichuan Province (2022YFS0597) and Electronic University of Science and Technology School of Medicine Clinical Medicine Discipline Development Fund（YXYLCJJ202402015）. Y.Z.L. discloses support for the research of this work from the Department of Science and Technology of Sichuan

Province (2025ZNSFSC1743).

Author contributions

L.Y. ,W.D. L. and H.S.J. conceptualized the project. L.Y., H.S.J., Z.Y.W. and J.Y. contributed to experimental design and data interpretation. Y.T., Z.H.L., Q.T and F.W. performed experiments and analyzed data helped by X.M.C., J.L.X., Q.T. Y.Z.L.,Y.Q.H. ,K.F.W. and M.J.L., L.Y. and Y.T. wrote the manuscript with input from all the authors. L.Y., W.D.L and H.S.J. and supervised the project, provided resources and acquired funds.

Declarations of interest

The authors declare no competing interests.

References

1 Jiang, X. *et al.* The role of m6A modification in the biological functions and diseases. *Signal Transduct Target Ther* **6**, 74, doi:10.1038/s41392-020-00450-x (2021).

2 Meyer, K. D. *et al.* Comprehensive analysis of mRNA methylation reveals enrichment in 3' UTRs and near stop codons. *Cell* **149**, 1635-1646, doi:10.1016/j.cell.2012.05.003 (2012).

3 Richard, E. M. *et al.* Bi-allelic Variants in METTL5 Cause Autosomal-Recessive Intellectual Disability and Microcephaly. *Am J Hum Genet* **105**, 869-878, doi:10.1016/j.ajhg.2019.09.007 (2019).

4 Weng, Y. L. *et al.* Epitranscriptomic m(6)A Regulation of Axon Regeneration in the Adult Mammalian Nervous System. *Neuron* **97**, 313-325 e316, doi:10.1016/j.neuron.2017.12.036 (2018).

5 Zhang, L. *et al.* Sevoflurane impairs m6A-mediated mRNA translation and leads to fine motor and cognitive deficits. *Cell Biol Toxicol* **38**, 347-369, doi:10.1007/s10565-021-09601-4 (2022).

6 Liu, C. & Kaeser, P. S. Mechanisms and regulation of dopamine release. *Curr Opin Neurobiol* **57**, 46-53, doi:10.1016/j.conb.2019.01.001 (2019).

7 Berke, J. D. What does dopamine mean? *Nature neuroscience* **21**, 787-793, doi:10.1038/s41593-018-0152-y (2018).

8 Bai, L. *et al.* m6A Demethylase FTO Regulates Dopaminergic Neurotransmission Deficits Caused by Arsenite. *Toxicol Sci* **165**, 431-446, doi:10.1093/toxsci/kfy172 (2018).

9 Hess, M. E. *et al.* The fat mass and obesity associated gene (Fto) regulates activity of the dopaminergic midbrain circuitry. *Nature neuroscience* **16**, 1042-1048, doi:10.1038/nn.3449 (2013).

10 Yu, Z. *et al.* Analysis of m6A modification regulators in the substantia nigra and striatum of MPTP-induced Parkinson's disease mice. *Neurosci Lett* **791**, 136907, doi:10.1016/j.neulet.2022.136907 (2022).

11 Teng, Y. *et al.* Conditional deficiency of m6A methyltransferase Mettl14 in substantia nigra alters dopaminergic neuron function. *J Cell Mol Med* **25**, 8567-8572, doi:10.1111/jcmm.16740 (2021).

12 Chen, X. *et al.* Down-Regulation of m6A mRNA Methylation Is Involved in Dopaminergic Neuronal Death. *ACS chemical neuroscience* **10**, 2355-2363, doi:10.1021/acschemneuro.8b00657 (2019).

13 Selberg, S. *et al.* Small-Molecule Inhibitors of the RNA M6A Demethylases FTO Potently Support the Survival of Dopamine Neurons. *International journal of molecular sciences* **22**, doi:10.3390/ijms22094537 (2021).

14 He, H. *et al.* METTL14 is decreased and regulates m(6) A modification of alpha-synuclein in Parkinson's

disease. *Journal of neurochemistry*, doi:10.1111/jnc.15882 (2023).

15 Li, H. B. *et al.* m(6)A mRNA methylation controls T cell homeostasis by targeting the IL-7/STAT5/SOCS pathways. *Nature* **548**, 338-342, doi:10.1038/nature23450 (2017).

16 Smidt, M. P., Smits, S. M. & Burbach, J. P. Molecular mechanisms underlying midbrain dopamine neuron development and function. *Eur J Pharmacol* **480**, 75-88, doi:10.1016/j.ejphar.2003.08.094 (2003).

17 Reddy, S. D. *et al.* Multiple coregulatory control of tyrosine hydroxylase gene transcription. *Proceedings of the National Academy of Sciences of the United States of America* **108**, 4200-4205, doi:10.1073/pnas.1101193108 (2011).

18 Mishra, A. K. & Dixit, A. Dopaminergic Axons: Key Recitalists in Parkinson's Disease. *Neurochem Res* **47**, 234-248, doi:10.1007/s11064-021-03464-1 (2022).

19 O'Keeffe, G. W. & Sullivan, A. M. Evidence for dopaminergic axonal degeneration as an early pathological process in Parkinson's disease. *Parkinsonism Relat Disord* **56**, 9-15, doi:10.1016/j.parkreldis.2018.06.025 (2018).

20 Brichta, L. *et al.* Identification of neurodegenerative factors using translatome-regulatory network analysis. *Nat Neurosci* **18**, 1325-1333, doi:10.1038/nn.4070 (2015).

21 Hossain, M. B., Islam, M. K., Adhikary, A., Rahaman, A. & Islam, M. Z. Bioinformatics Approach to Identify Significant Biomarkers, Drug Targets Shared Between Parkinson's Disease and Bipolar Disorder: A Pilot Study. *Bioinform Biol Insights* **16**, 11779322221079232, doi:10.1177/11779322221079232 (2022).

22 Hobson, B. D. *et al.* Subcellular and regional localization of mRNA translation in midbrain dopamine neurons. *Cell Rep* **38**, 110208, doi:10.1016/j.celrep.2021.110208 (2022).

23 Shu, L., Huang, X., Cheng, X. & Li, X. Emerging Roles of N6-Methyladenosine Modification in Neurodevelopment and Neurodegeneration. *Cells* **10**, doi:10.3390/cells10102694 (2021).

24 Mathoux, J., Henshall, D. C. & Brennan, G. P. Regulatory Mechanisms of the RNA Modification m(6)A and Significance in Brain Function in Health and Disease. *Front Cell Neurosci* **15**, 671932, doi:10.3389/fncel.2021.671932 (2021).

25 Zhang, N., Ding, C., Zuo, Y., Peng, Y. & Zuo, L. N6-methyladenosine and Neurological Diseases. *Mol Neurobiol* **59**, 1925-1937, doi:10.1007/s12035-022-02739-0 (2022).

26 Shi, H. *et al.* m(6)A facilitates hippocampus-dependent learning and memory through YTHDF1. *Nature* **563**, 249-253, doi:10.1038/s41586-018-0666-1 (2018).

27 Widagdo, J. *et al.* Experience-Dependent Accumulation of N6-Methyladenosine in the Prefrontal Cortex Is Associated with Memory Processes in Mice. *J Neurosci* **36**, 6771-6777, doi:10.1523/JNEUROSCI.4053-15.2016 (2016).

28 Li, L. *et al.* Fat mass and obesity-associated (FTO) protein regulates adult neurogenesis. *Hum Mol Genet* **26**, 2398-2411, doi:10.1093/hmg/ddx128 (2017).

29 Zhang, Z. *et al.* METTL3-mediated N(6)-methyladenosine mRNA modification enhances long-term memory consolidation. *Cell research* **28**, 1050-1061, doi:10.1038/s41422-018-0092-9 (2018).

30 Wang, Y. *et al.* N(6)-methyladenosine RNA modification regulates embryonic neural stem cell self-renewal through histone modifications. *Nature neuroscience* **21**, 195-206, doi:10.1038/s41593-017-0057-1 (2018).

31 Yoon, K. J. *et al.* Temporal Control of Mammalian Cortical Neurogenesis by m(6)A Methylation. *Cell* **171**, 877-889 e817, doi:10.1016/j.cell.2017.09.003 (2017).

32 Xu, H. *et al.* m(6)A mRNA Methylation Is Essential for Oligodendrocyte Maturation and CNS Myelination. *Neuron* **105**, 293-309 e295, doi:10.1016/j.neuron.2019.12.013 (2020).

33 Koranda, J. L. *et al.* Mettl14 Is Essential for Epitranscriptomic Regulation of Striatal Function and Learning. *Neuron* **99**, 283-292 e285, doi:10.1016/j.neuron.2018.06.007 (2018).

34 Chemaly, E. R., Troncone, L. & Lebeche, D. SERCA control of cell death and survival. *Cell Calcium* **69**, 46-61, doi:10.1016/j.ceca.2017.07.001 (2018).

35 Dahl, R. A new target for Parkinson's disease: Small molecule SERCA activator CDN1163 ameliorates dyskinesia in 6-OHDA-lesioned rats. *Bioorg Med Chem* **25**, 53-57, doi:10.1016/j.bmc.2016.10.008 (2017).

36 Hetz, C. & Saxena, S. ER stress and the unfolded protein response in neurodegeneration. *Nat Rev Neurol* **13**, 477-491, doi:10.1038/nrneurol.2017.99 (2017).

37 Ghemrawi, R. & Khair, M. Endoplasmic Reticulum Stress and Unfolded Protein Response in Neurodegenerative Diseases. *Int J Mol Sci* **21**, doi:10.3390/ijms21176127 (2020).

38 Kong, Y. *et al.* METTL3 mediates osteoblast apoptosis by regulating endoplasmic reticulum stress during LPS-induced inflammation. *Cell Signal* **95**, 110335, doi:10.1016/j.cellsig.2022.110335 (2022).

39 Du, Q. Y. *et al.* METTL3 potentiates progression of cervical cancer by suppressing ER stress via regulating m6A modification of TXNDC5 mRNA. *Oncogene* **41**, 4420-4432, doi:10.1038/s41388-022-02435-2 (2022).

40 Dou, X. *et al.* METTL14 is a chromatin regulator independent of its RNA N6-methyladenosine methyltransferase activity. *Protein & cell* **14**, 683-697, doi:10.1093/procel/pwad009 (2023).

41 Wei, J. *et al.* HRD1-mediated METTL14 degradation regulates m(6)A mRNA modification to suppress ER proteotoxic liver disease. *Mol Cell* **81**, 5052-5065 e5056, doi:10.1016/j.molcel.2021.10.028 (2021).

42 Cao, X. *et al.* Mettl14-Mediated m(6)A Modification Facilitates Liver Regeneration by Maintaining Endoplasmic Reticulum Homeostasis. *Cell Mol Gastroenterol Hepatol* **12**, 633-651, doi:10.1016/j.jcmgh.2021.04.001 (2021).

43 Zhang, X. *et al.* Deubiquitinase USP19 modulates apoptotic calcium release and endoplasmic reticulum stress by deubiquitinating BAG6 in triple negative breast cancer. *Clin Transl Med* **13**, e1398, doi:10.1002/ctm2.1398 (2023).

44 Wang, J. *et al.* WTAP promotes myocardial ischemia/reperfusion injury by increasing endoplasmic reticulum stress via regulating m(6)A modification of ATF4 mRNA. *Aging (Albany NY)* **13**, 11135-11149, doi:10.18632/aging.202770 (2021).

45 Subbarayalu, P. *et al.* The RNA Demethylase ALKBH5 Maintains Endoplasmic Reticulum Homeostasis by Regulating UPR, Autophagy, and Mitochondrial Function. *Cells* **12**, doi:10.3390/cells12091283 (2023).

46 Liu, C. *et al.* ALKBH5 protects against stroke by reducing endoplasmic reticulum stress-dependent inflammation injury via the STAT5/PERK/EIF2alpha/CHOP signaling pathway in an m(6)A-YTHDF1-dependent manner. *Exp Neurol* **372**, 114629, doi:10.1016/j.expneurol.2023.114629 (2024).

47 He, M., Li, D., Fang, C. & Xu, Q. YTHDF1 regulates endoplasmic reticulum stress, NF-kappaB, MAPK and PI3K-AKT signaling pathways in inflammatory osteoclastogenesis. *Arch Biochem Biophys* **732**,

109464, doi:10.1016/j.abb.2022.109464 (2022).

48 Shi, J. *et al.* Cleavage of GSDMD by inflammatory caspases determines pyroptotic cell death. *Nature* **526**, 660-665, doi:10.1038/nature15514 (2015).

49 Lei, H. *et al.* METTL3 induces bone marrow mesenchymal stem cells osteogenic differentiation and migration through facilitating M1 macrophage differentiation. *Am J Transl Res* **13**, 4376-4388 (2021).

50 Fricker, M., Tolkovsky, A. M., Borutaite, V., Coleman, M. & Brown, G. C. Neuronal Cell Death. *Physiol Rev* **98**, 813-880, doi:10.1152/physrev.00011.2017 (2018).

51 Yan, Q. *et al.* Transcriptomic reveals the ferroptosis features of host response in a mouse model of Zika virus infection. *J Med Virol* **95**, e28386, doi:10.1002/jmv.28386 (2023).

52 Lakhal-Littleton, S. *et al.* Cardiac ferroportin regulates cellular iron homeostasis and is important for cardiac function. *Proceedings of the National Academy of Sciences of the United States of America* **112**, 3164-3169, doi:10.1073/pnas.1422373112 (2015).

Figure legends

Fig1. Increased impairment of behavior function in Mettl14-cKO mice with aging

(A) Schematic diagram of the mice behavioral test. (B) Latency to fall from the accelerating rotarod in mice of different ages. (C) Latency to fall from the accelerating rotarod in nine months old mice; mice were given 5 trials per day. (D) Each data point represents the average of 5 trials per training session in (C). (E) Time in pole test of mice at different ages. (F) Time in pole test in nine months old mice; mice were given 5 trials per day. (G) Time in pole test in nine months old mice; each data point represents the average of 5 trials per training session. (H) Representative diagram of Mettl14-cKO and Ctrl mice movement trajectory in the open field test. (I-K) Time the mice spent, distance the mice moved, and the number of entries in the center zone of the open field. (L) Representative diagram of Mettl14-cKO and Ctrl mice movement trajectory in the plus maze. (M-O) Time the mice spent in the opened arm, distance the mice moved in the opened arm, and resting time the mice stayed in the closed arm of the plus maze. All data are presented as mean ± SD (4-9 mice per group), ns indicated no significant, * $P < 0.05$, ** $P < 0.01$ compared with Ctrl.

Fig2. Deletion of Mettl14 leads to progressive degeneration of DA neurons in Mettl14-cKO mice

(A) Mesencephalic sections were stained with anti-tyrosine hydroxylase and counterstained with Nissl. TH and Nissl positive cells in VTA region were counted in sections obtained from WT and cKO mice. Stereological cell counts of TH-immunoreactive cells in the SNpc region of WT and cKO mice, Scale bar represents 200 μM.(B) Quantification of TH+ neuron in VTA region and SN region in WT and cKO mice (n=5). (C) TH, PITX3, and NURR1 expression in the substantia nigra of Mettl14-cKO and Ctrl mice were detected by WB assay. (D) Quantification of WB. Protein expression is normalized to β-actin, the quantitative data represent the relative values compared to the control group. (E) Dopamine transmitter level in the substantia nigra of Mettl14-cKO and Ctrl mice detected by ELISA assay. (F-G) A representative diagram of Golgi staining in SN of Mettl14-cKO and Ctrl mice (bar=200 μm or 5 μm). (H-L) Quantification shows spine number in SN neurons (22–31 random dendrites from 4 mice were analyzed). All data are

presented as mean ± SD, ns indicated no significant, * $P < 0.05$, ** $P < 0.01$ compared with Ctrl.

Fig3. Alteration m6A methylation and gene transcription profile in SN region of Mettl14-cKO mice

(A) m6A peak density analysis in different genomic region. (B) Transcripme-wide distribution of m6A peaks in Mettl14-cKO and Ctrl mice, respectively. (C) The number of differential genes obtained by comparing m6A peak density between Mettl14-cKO and Ctrl mice. (D) Consensus motif of differential m6A sites between Mettl14-cKO and Ctrl mice. (E) The volcano plot illustrates the differential genes between Mettl14-cKO and Ctrl mice in mRNA sequencing. (F) Heat map displays the top 30 differential genes between Mettl14-cKO and Ctrl mice in mRNA sequencing. (G) Based on the analysis of genes involved in Biological Process (BP), Cellular Component (CC), and Molecular Function (MF), the gene ontology (GO) analysis reveals significant pathways altered between Mettl14-cKO and control mice as identified through mRNA sequencing.

Fig4. METTL14-mediated m6A modification impacts *Atp2a3* expression

(A) The volcano map illustrates the intersection of differential genes in mRNA and m6A-MeRIP sequencing. (B) The Venn diagram analyzed hypo-down genes enriched in both GO and KEGG analysis and intersected them with those genes that are highly expressed in DA neurons (from the GEO database). Three genes were highlighted. (C) mRNA and m6A reads profiles of Atp2a3, Neurod1, and Pomc in Mettl14-cKO and Ctrl mice from mRNA and MeRIP sequencing. (D) Schematic diagram of m6A modification sites on human *Atp2a3* mRNA. (E) SH-SY5Y cells were transfected with an empty pCRIPERV2 vector (NC) or two pCRIPERV2-gRNA plasmids (Mettl14-KD#1 and Mettl14-KD#2). Forty-eight hours later, METTL14 protein expression was detected by WB assay (Con: SH-SY5Y cells without transfection) and (F) Quantification. (G) Cells were transfected with the pCRIPERV2 vector (NC) or pCRIPERV2-gRNA plasmids. *Atp2a3* mRNA expression in NC or Mettl14-KD SH-SY5Y cells was detected by RT-qPCR. (H) SH-SY5Y cells were treated the same as (F), MeRIP assay was conducted to detect the m6A level on site-427 and site-1118 of *Atp2a3* mRNA. (I-J) Schematic diagram of double luciferase reporter plasmid construction. (K) The translation efficiency of *Atp2a3* is defined as the quotient of reporter protein production (F-luc/R-luc). All data are presented as mean ± SD, ns indicated no significant, * $P < 0.05$, ** $P < 0.01$ compared to NC.

Fig5 Deficiency of Mettl14 disturbs calcium imbalance and triggers ER stress

(A-B) SH-SY5Y cells were transfected with an empty pCRIPERV2 vector (NC) or pCRIPERV2-gRNA plasmids (Mettl14-KD#1 and Mettl14-KD#2), 12 hours later, cellular Ca^{2+} was detected by FLUO-3 AM probe and flow cytometry. (C) SH-SY5Y cells were treated the same as (A), 12 hours later, cellular Ca^{2+} was observed under microscope (bar=10μm). (D) The endoplasmic reticulum and mitochondria of neurons in SN of Ctrl and Mettl14-cKO mice were observed under a transmission electron microscope (bar=1μm left or 500nm right). (E-F) The distance between ER and outer mitochondrial membrane (OMM) and the number of ER-Mito contacts per 10 μm Mitochondrial membrane surface were analyzed (n=4). (G)SH-SY5Y cells were treated the same as (A), 12 or 24 hours later, ER stress marker proteins GRP78, ATF4 and

CHOP expression were detected by WB assay. (H-J) Quantification of WB. All data are presented as mean ± SD, ns indicated no significant, * $P < 0.05$, ** $P < 0.01$ compared to NC.

Fig6. Deficiency of Mettl14 renders cells susceptible to cell death

SH-SY5Y cells were transfected with an empty pCRIPERV2 vector (NC) or pCRIPERV2-gRNA plasmids (Mettl14-KD#1 and Mettl14-KD#2), the cellular ROS and cell death were detected. (A-B) 12 hours after transfection, cells were treated DCFH-DA for 15 min and the cellular ROS was detected by flowcytometry. (C) Cells were treated the same with (A-B), cellular ROS was observed under microscope (bar=10μm). (D) Relative cell number of the NC and Mettl14-KD groups was quantified by cell counting 24 hours after transfection. (E-K) Cells were stained with Annexin V and Prodium Iodide (PI), the alive and dead cells were detected by flow cytometry and microscope. The percentage of alive cells (negative cells, E-F), the percentage of Annexin V-positive cells (G-H), and the percentage of PI-positive cells (I-J) were quantified. (K) Fluorescent images visually show that the Annexin V- and PI-positive cells are increased in the Mettl14-KD group compared to NC. All data are presented as mean ±SD, ** $P < 0.01$ compared to NC.

Fig7. Atp2a3 overexpression reverses ER stress and cell death in Mettl14-deficiency cells

(A-B) SH-SY5Y cells were transfected with pCRIPERV2-gRNA#1 plasmid (Mettl14-KD) or pCMV-Atp2a3-cDNA coding plasmid (Atp2a3-OE), combined with their empty vectors (Control: cells were transfected with empty pCRIPERV2 and empty pCMV vectors; Mettl14-KD: cells were transfected with pCRIPERV2-gRNA#1 and empty pCMV vector; KD&Atp2a3-OE: cells were transfected with pCRIPERV2-gRNA#1 and pCMV-Atp2a3-cDNA coding plasmid). 12 hours later, cellular Ca^{2+} was detected by FLUO-3 AM probe and flow cytometry. (C) SH-SY5Y cells were treated the same as (A), 12 hours later, ER stress marker proteins GRP78, ATF4 and CHOP expression were detected by WB assay. (D-F) Quantification of WB. (G-H) SH-SY5Y cells were treated the same as (A), 12 hours later, cells were treated DCFH-DA for 15 min and the cellular ROS was detected by flowcytometry. The mean DCF fluorescence intensity were quantified as relative DCFH-DA DCFH-DA level. (I) SH-SY5Y cells were treated the same as (A), 24 hours later, Relative cell number was quantified by cell counting assay. All data are presented as mean ±SD. * $P < 0.05$, ** $P < 0.01$ compared to Control; $^{\#\#}$ $P < 0.01$ compared to Mettl14-KD.

Fig8. Restoring *Mettl14* rescues PD-like phenotype in Mettl14-cKO mice

(A) Schematic diagram of mice treatment and behavioral test. Lentivirus expressing Mettl14 (Lenti-Mettl14) was intracerebrally injected into the SN of 8-12 weeks old Mettl14-cKO mice to recover METTL14 expression. Lenti-NC (without Mettl14 expression sequence) was injected as a control. The behavioral function was tested at 7-9 months old age. (B) The expression of METTL14 and DAT in the SN of cKO/Lenti-NC and cKO/Lenti-Mettl14 mice was detected by immunofluorescence (bar=10μm). (C) Latency to fall from the accelerating rotarod in mice of 7-9 months old age. (D) Latency to fall from the accelerating rotarod in 7-9 months old mice, mice were given 5 trials per day. (E) Latency to fall from the accelerating rotarod in 7-9 months old mice, each data point represents the average of 5 trials per training

session. (F) Time in the pole test in mice of 7-9 months old age. (G) Time in the pole test in 7-9 months old mice, mice were given 5 trials per day. (H) Time in the pole test in 7-9 months old mice, each data point represents the average of 5 trials per training session (n=8). (I) The staining of TH in SN of Ctrl/Lenti-NC, Mettl14-cKO/Lenti-NC, and Mettl14-cKO/Lenti-Mettl14 mice by IF assay (bar=150μm or 30μm). (J) Quantification of TH-positive cell numbers from (I), 6 slices from 3 mice per group. All data are presented as mean ± SD, ** $P < 0.01$ compared to Ctrl/Lenti-NC; $^{\#}P < 0.05$ and $^{\#\#}P < 0.01$ compared to Mettl14-cKO/Lenti-NC.